ELSEVIER

Tectonophysics 307 (1999) 135–162

TECTONOPHYSICS

www.elsevier.com/locate/tecto

Magnetic fabric constraints on the initial geometry of the Sudbury Igneous Complex: a folded sheet or a basin-shaped igneous body?

E. Jun Cowan *

Department of Geology, University of Toronto, Toronto, ON M5S 3B1, Canada

Accepted 31 March 1999

Abstract

Interpreted either as a folded igneous sheet or a basin-shaped intrusion, the origin of the Palaeoproterozoic Sudbury Igneous Complex (SIC), Ontario, Canada, has been debated by geologists for over a century. Most recent proposals view the SIC to have been emplaced as a horizontal impact melt and subsequently folded after solidification. This requires the SIC to have folded from an originally horizontal sheet, to the present basinal geometry, with dips of 30° in the North Range and 70° in the East Range. The fold scenario would require the sharply curved juncture between the North and East Ranges (North Lobe) to be deformed in the solid-state due to folding. In order to test the fold model, the rock fabric was investigated in the East and North Ranges and the North Lobe of SIC at 256 sites with the aid of anisotropy of magnetic susceptibility (AMS). A sampling transect through an undeformed portion of the SIC in the western North Range reveals that the gabbro–norite exhibits SIC contact-parallel magnetic foliation and down-dip magnetic lineation, both of which, respectively, correlate to an igneous foliation and lineation. The granophyre, in contrast, features spatially consistent magnetic lineation that is oriented orthogonal to the SIC contact. This magnetic lineation can be correlated to a mineral fabric characterised by aligned acicular crystals of plagioclase, and is interpreted to be a wall-orthogonal crystallisation texture. The East and North Ranges in the eastern SIC reveal similar patterns of AMS fabrics. The magnetic lineation of the granophyre is orthogonal to the basal contact of the SIC in the East and North Ranges, and in the fold-like North Lobe between the two ranges. An axial-planar magnetic foliation is developed in the granophyre as the North Lobe is approached, but the magnetic lineation is nevertheless contact-orthogonal and well-defined. This AMS fabric is interpreted to be a combination of an original igneous contact-orthogonal lineation and a foliation resulting from tectonic overprint. The preservation of the contact-orthogonal magnetic lineation implies low levels of tectonic overprint. Conservative shortening strains estimated from AMS numerical modelling suggest <15% strain in the North Lobe, but most likely <5% strain, as judged from the paucity of microstructural evidence for solid-state deformation. Such low levels of strain are more consistent with a basin-shaped intrusive origin for the SIC, rather than folding of an initially horizontal, and consolidated igneous sheet. This rules out models of initial horizontal sheet emplacement including the recently proposed impact-melt model for the SIC.

Keywords: Sudbury Igneous Complex; AMS; fabric; structure; intrusion; impact; meteorite

* E-mail: juncowan@yahoo.com. Present address: SRK Consulting, 25 Richardson Street, West Perth, WA 6005, Australia.

0040-1951/99/$ – see front matter
PII: S0040-1951(99)00123-7

1. Introduction

The Sudbury Basin comprises a 1.85 Ga layered norite–gabbro–granophyre sequence known as the *main mass* of the Sudbury Igneous Complex (SIC), and the Whitewater Group, which in vertical succession is subdivided into the Onaping, Onwatin and Chelmsford Formations (Fig. 1). The main mass of the SIC is underlain by a discontinuous sulphide-rich noritic unit called the Sublayer, and radial and concentrically oriented quartz dioritic Offset Dykes extend out from the SIC into the basement lithologies. Geological features such as shatter cones, pseudotachylytes, and planar deformation lamellae in quartz and zircon, are documented from the Archaean and Proterozoic Superior and Southern Province basement lithologies surrounding the 60×27 km elliptical Sudbury Basin (Dietz, 1964; Dietz and Butler, 1964; Krogh et al., 1984, 1996; Lakomy, 1990; Dressler et al., 1991; Spray and Thompson, 1995). The presence of these features in the basement rocks is consistent with shock-induced deformation associated with the hypervelocity impact of an extraterrestrial mass.

In addition to the shock metamorphic structures, previous work has shown that impact melts may be preserved in the Onaping Formation (Peredery, 1972; Peredery and Morrison, 1984; Dressler et al., 1996), a heterolithic deposit interpreted as an impact-generated fall-back breccia, or a pseudovolcanic succession of impact-induced hydroclastic and pyroclastic deposits, comprised almost entirely of brecciated and locally derived Archaean and Proterozoic lithologies (Avermann, 1994; Ames and Gibson, 1995). More recent studies suggest that the SIC, an igneous body with high levels of crustal contamination, is consistent with impact melting (Faggart et al., 1985; Grieve et al., 1991). Grieve et al. (1991) interpreted the SIC to have differentiated into its tripartite composition by in-situ fractionation in an impact-generated melt-lake. The impact-melt model for the SIC consequently constrains the initial geometry of the SIC to a horizontal sheet (Cowan and Schwerdtner, 1994), because an impact melt, in the order of kilometres in thickness, can only form from a large impact that results in a *complex crater* with a horizontal floor (Cintala and Grieve, 1994). The impact-melt hypothesis for the SIC, thus excludes magma geometries and emplacement scenarios previously thought relevant to the SIC, such as a lopolithic intrusion (Hamilton, 1960; Peredery and Morrison, 1984).

Although the southern half of the SIC is transected by a 5 km thick strain belt known as the South Range shear zone (Fig. 1b; Shanks and Schwerdtner, 1991), the SIC is reported to be unaffected by tectonic deformation elsewhere, particularly in the East and North Ranges of the Sudbury Basin (Muir, 1984; Rousell, 1984). This seems incompatible with the impact-melt model for the SIC. The folding of an initially horizontal, and solidified impact-melt sheet, to present dips of 30° to 70°, in the North and East Ranges, respectively (Fig. 1), requires solid-body rotations of the fold-limbs. Such rotations must be accompanied with solid-state distortion at the fold bends. The strain levels at the sharp bends of the SIC are judged as very low (e.g., Dressler, 1987), but have not been estimated quantitatively. The aim of the present study is to quantify the strain intensities in SIC phases exposed along the East and North Ranges of the Sudbury Basin, and compare these estimates to strains expected for the folding of a solidified igneous sheet.

Tectonic strain fabrics of low-strain igneous rocks are difficult to analyse. In order to overcome this difficulty, the anisotropy of magnetic susceptibility (AMS) is used in this study to document the magnetic subfabric of the total rock fabric. For strained igneous rocks exhibiting little or no evidence of solid-state deformation, the magnetic subfabric is a combination of the crystallisation fabric formed during the cooling of the igneous body and a superposed solid-state strain. The original igneous fabric is destroyed only if the imposed strain is substantial, otherwise the original igneous fabric can be detected with the AMS (Richter, 1992). The degree of strain required to modify, and

Fig. 1. Location map and geological setting. (a) Simplified geological map of the Sudbury Basin, with the study areas marked with boxes. (b) Block diagram of the eastern Sudbury Basin. Cross-section is based on the Lithoprobe seismic profile (Milkereit et al., 1992), and structural data on the horizontal surface is based on Cowan (1996). Y-shaped arrows indicate sedimentary younging directions. Tectonic foliation trajectories shown in the plane of cross-section is inferred.

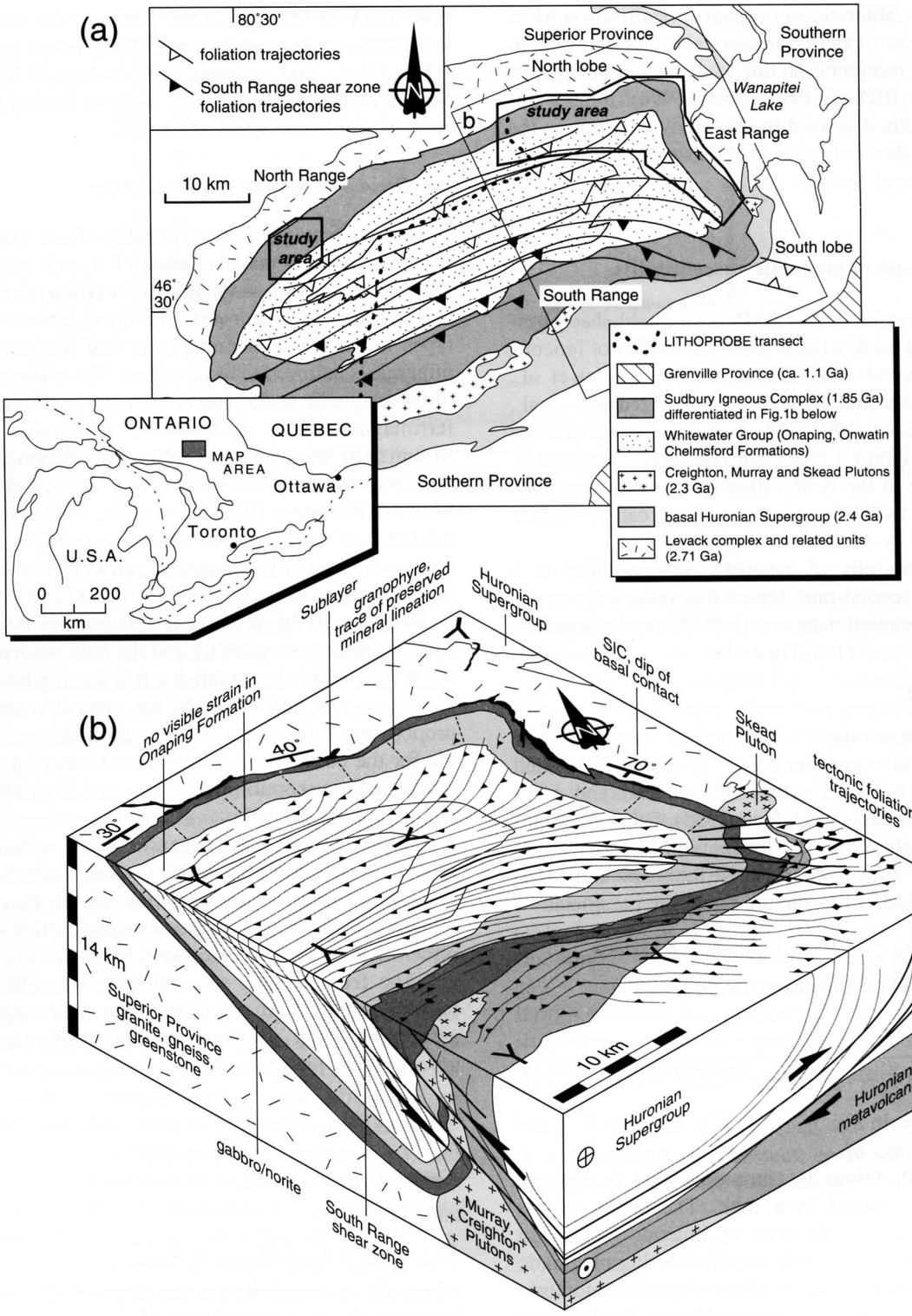
(a)
80°30'
foliation trajectories
South Range shear zone foliation trajectories
Superior Province
Southern Province
North lobe
Wanapitei Lake
study area
East Range
b
10 km
North Range
study area
South lobe
46° 30'
South Range
Southern Province
ONTARIO
QUEBEC
MAP AREA
Ottawa
Toronto
U.S.A.
0 200 km
LITHOPROBE transect
Grenville Province (ca. 1.1 Ga)
Sudbury Igneous Complex (1.85 Ga) differentiated in Fig.1b below
Whitewater Group (Onaping, Onwatin Chelmsford Formations)
Creighton, Murray and Skead Plutons (2.3 Ga)
basal Huronian Supergroup (2.4 Ga)
Levack complex and related units (2.71 Ga)
(b)
Sublayer
granophyre, trace of preserved mineral lineation
Huronian Supergroup
SIC, dip of basal contact
no visible strain in Onaping Formation
40°
70°
Skead Pluton
tectonic foliation trajectories
30°
14 km
Superior Province granite, gneiss, greenstone
10 km
Huronian Supergroup
Huronian metavolcanics
gabbro/norite
South Range shear zone
Murray, Creighton Plutons

eventually obliterate, an original crystallisation AMS fabric can be modelled numerically, assuming magnetic grain reorientation due to distortion of the host rock mass (Richter, 1992; Benn, 1994). Such a numerical method is used in this study to estimate the amount of shortening strain consistent with the magnetic fabrics of the SIC.

2. Anisotropy of magnetic susceptibility

The determination of AMS is an established physical method used in the petrofabric studies of igneous rocks (Ellwood and Whitney, 1980; Guillet et al., 1983; Cruden and Launeau, 1994; Archanjo et al., 1995; Bouchez, 1997). Magmatic lineations and foliations of igneous rocks are commonly not readily measurable in the field, either due to exposure conditions or low fabric anisotropies, but can be rapidly established by AMS measurements.

The anisotropy of magnetic susceptibility is a symmetric second-rank tensor that relates the intensity of the applied magnetic field (H) to the acquired magnetization (M) of a material:

$$M_i = \mathbf{K}_{ij} H_j \tag{1}$$

The dimensionless susceptibility tensor $\mathbf{K}_{ij}$ has the principal components $K_1 \geq K_2 \geq K_3$ which correspond to the principal radii of a triaxial AMS ellipsoid (Hrouda, 1982; Nye, 1985). Other AMS parameters (Jelinek, 1978; Tarling and Hrouda, 1993) used in this study to characterise the shape and intensity of the AMS ellipsoid are the shape parameter:

$$T = \left[2(\ln K_2 - \ln K_3)/(\ln K_1 - \ln K_3)\right] - 1$$

and the modified anisotropy degree:

$$P' = \exp\sqrt{\left\{2\left[(\eta_1 - \eta_m)^2 + (\eta_2 - \eta_m)^2 + (\eta_3 - \eta_m)^2\right]\right\}}$$

where $\eta_1 = \ln K_1$; $\eta_2 = \ln K_2$; $\eta_3 = \ln K_3$; and $\eta_m = \sqrt[3]{\eta_1 \cdot \eta_2 \cdot \eta_3}$.

The AMS fabric is commonly due to mineral preferred alignment in a rock. The origin of the mineral fabric, in the case of igneous rocks, can be entirely due to a fabric acquired during magmatic crystallisation, or a combination of igneous subfabric with a superposed solid-state subfabric. Deciphering how much of the total AMS fabric is the result of solid-state strain, can be done if the initial igneous AMS fabric and magnetic mineralogy is known. Such a method is used in this study to determine the level of solid-state strain of the SIC.

2.1. Source of magnetic susceptibility

Low-field magnetic susceptibility (K_{LF}) measures the bulk-induced magnetisation of a rock resulting from diamagnetic, paramagnetic, antiferromagnetic, and ferrimagnetic minerals. In most igneous rock types the effect of paramagnetic and ferrimagnetic minerals is believed to be dominant. The composition of the magnetic grains can be assumed to be entirely ferrimagnetic if the susceptibility values are $>10^{-2}$ SI units (Archanjo et al., 1995), while paramagnetic susceptibility values are not likely to exceed 10^{-3} SI units (Rochette, 1987; Benn et al., 1993). Various mixtures of ferrimagnetic and paramagnetic grains are expected to be the magnetic carriers for susceptibility values in the range 10^{-4} to 10^{-2} SI units.

Because of the non-linear relationship between ferrimagnetic susceptibility and the bulk susceptibility, it is desirable to establish a relationship between these two susceptibilities. In the present study, the proportion of ferrimagnetic susceptibility responsible for the bulk susceptibility was obtained by measuring bulk susceptibilities at low and high applied magnetic field strengths.

Magnetic susceptibility measurements at high applied field strengths (K_{HF}), that is, at strengths higher than the saturation magnetisation of ferrimagnetic minerals, measures the induced magnetisation of all minerals with the exclusion of ferrimagnetic minerals. The ferrimagnetic susceptibility, therefore, can be obtained by subtracting the high field magnetic susceptibility (K_{HF}) from the low field magnetic susceptibility (K_{LF}):

$$K_{ferri} = K_{LF} - K_{HF} \tag{2}$$

since:

$$K_{HF} = K_p + K_d + K_{aferro}$$

and

$$K_{LF} = K_p + K_d + K_{aferro} + K_{ferri}$$

where K_p = susceptibility due to paramagnetic behaviour; K_d = susceptibility due to diamagnetic

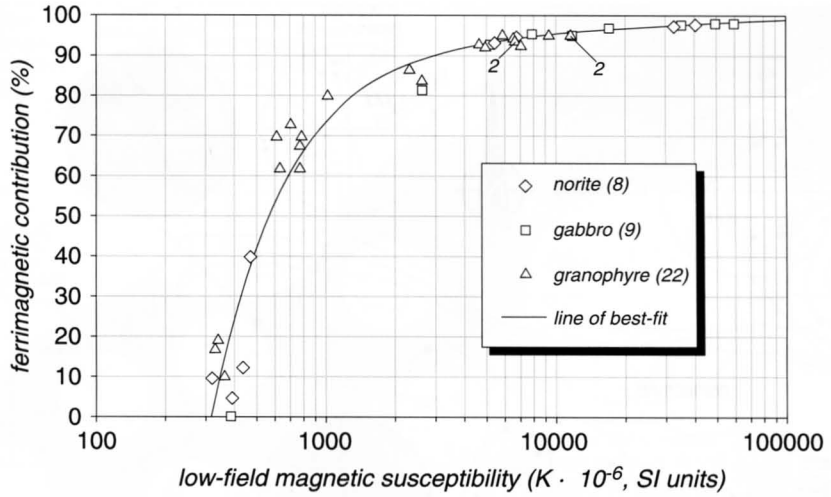

Fig. 2. Correlation curve between percentage ferrimagnetic contribution (K_{ferri}) to the bulk susceptibility measured at low field strengths (K_{LF}). The proportion of K_{ferri} is calculated from slope of the hysteresis curve at high field strengths (K_{HF}) over the initial slope at low fields (K_{LF}).

behaviour; K_{aferro} = susceptibility due to antiferromagnetic behaviour; and K_{ferri} = susceptibility due to ferrimagnetic behaviour (Richter et al., 1994; Richter and van der Pluijm, 1994; Rochette, 1994a).

The percentage K_{ferri} responsible for the magnetic susceptibility for all minerals (K_{LF}) can be thus calculated from the relationship of Eq. 2 (i.e., $K_{LF} - K_{HF}/K_{LF}$).

In the present study the low field AMS fabric is determined from core samples (2.2 cm long and 2.54 cm in diameter) using a Sapphire SI-2 induction coil instrument, with an applied field of 0.1 mT. Statistical site averaging of the magnetic fabric, orientation of the AMS tensor, P' and T values were computed using the matrix averaging routines of Hext (1963) and Jelinek (1978).

High field susceptibility (K_{HF}) measurements were conducted on selected samples of the SIC with a vibrating sample magnetometer, with applied fields of up to 0.7 T. Widely ranging susceptibility values of these samples allowed an empirical relationship between the low-field magnetic susceptibility and ferrimagnetic contribution to be established (shown graphically in Fig. 2). This relationship was then used to determine $\%K_{ferri}$ for the other sites where K_{HF} values were not measured. The relationship of Fig. 2 indicates that the SIC samples with susceptibility values of $<400 \times 10^{-6}$ was found to have less than 20% ferrimagnetic influence on the susceptibility.

The SIC samples were found to exhibit a wide range of susceptibility values that indicate a range of ferrimagnetic contribution (K_{ferri}) from 0% to nearly 100%. The relationship of Fig. 2 was used as a guide to investigate whether there is a perceptible difference between the magnetic fabric orientations obtained from predominantly ferrimagnetic carriers (in this case predominantly magnetite), or samples lacking in ferrimagnetic carriers (in this case inferred to be dominated by paramagnetic mineralogy of amphibole, ilmenite, chlorite and biotite). Magnetic fabrics from two neighbouring sample sites from the northeastern quadrant of the SIC (Fig. 1a) that contrast in susceptibilities are almost identical in magnetic lineation and foliation orientations (Fig. 3). The similarities observed in magnetic fabrics of neighbouring sites clearly establishes that the magnetic fabric *directions* are independent of the magnetic mineralogy.

3. 3. Onaping Falls transect: correlation of magnetic fabric with petrofabric

3.1. Magnetic fabrics

The AMS fabrics that result from an initial igneous fabric and a superposed tectonic strain may

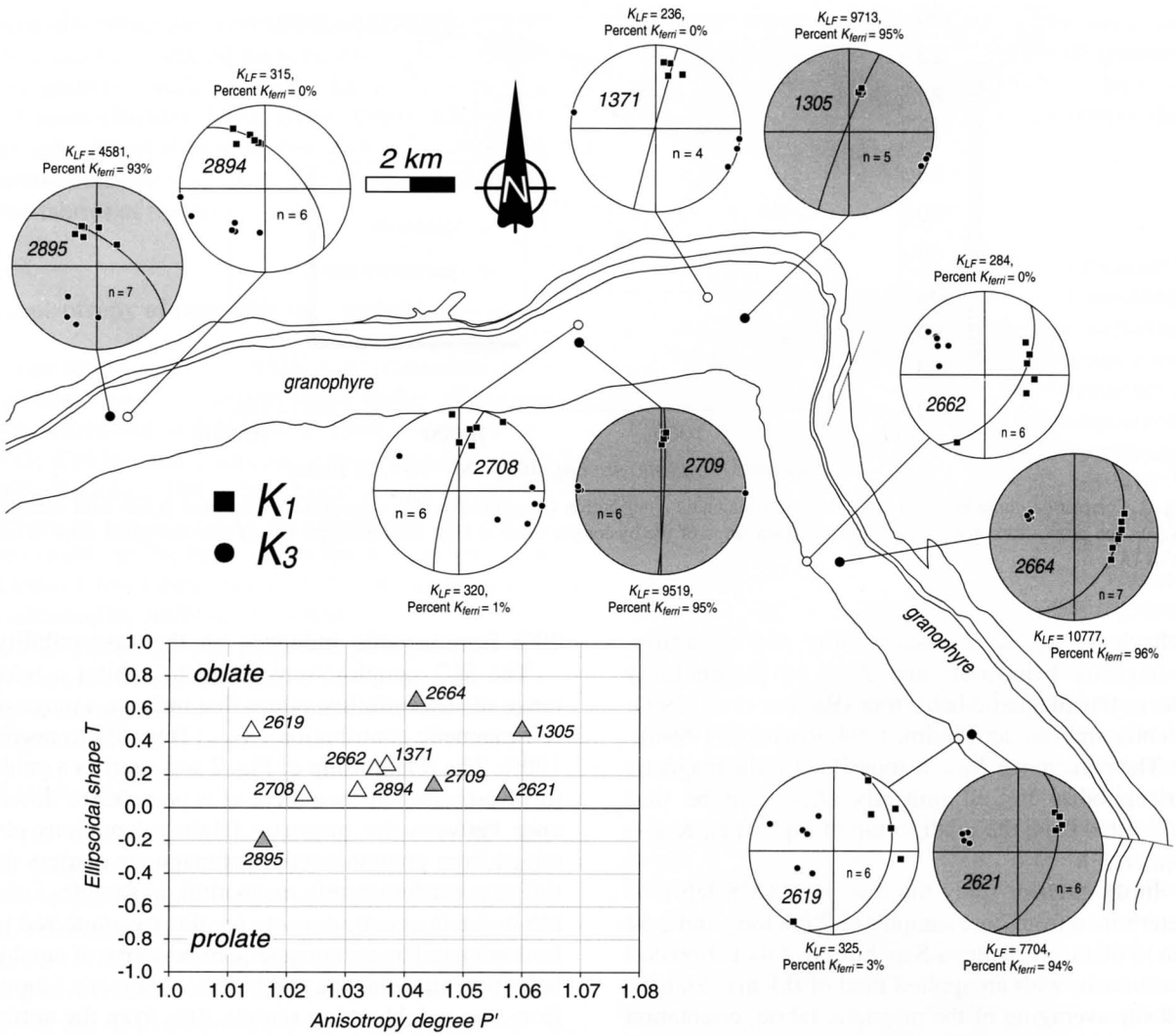

Fig. 3. Stereonets of AMS K_1 and K_3 directions from stations with contrasting susceptibility values. Low-field susceptibility values (K_{LF}) are in 10^{-6} SI units. Percent K_{ferri} are also indicated for each site obtained from the relationship of Fig. 2. White stereonets represent sites with low ferrimagnetic susceptibility (likely dominated by paramagnetic mineralogy), while the shaded nets are sites with almost 100% ferrimagnetic susceptibility. Great circles indicate the mean magnetic foliation. Site mean P' versus T plot is also shown for each of the sites.

be modelled numerically if: (1) the magnetic carriers are known; and (2) the preferred orientation of the magnetic minerals prior to deformation can be estimated (Richter, 1992; Benn, 1994). Once the magnetic carriers are identified, suitable ranges of intrinsic grain susceptibilities anisotropies (e.g., Borradaile, 1988; Tarling and Hrouda, 1993) can be used for the numerical modelling.

The pre-strain orientation distribution of magnetic carrier grains can be estimated if the unstrained AMS fabric can be determined with some confidence. A sampling transect along Highway 144 northeast of Windy Lake in the North Range of the SIC was selected to document the pre-strain fabric of the SIC lithologies because of the absence of tectonic strain in the adjacent Onaping Formation (western study area shown in Fig. 1a). Twelve, three and two oriented samples were obtained from granophyre, gab-

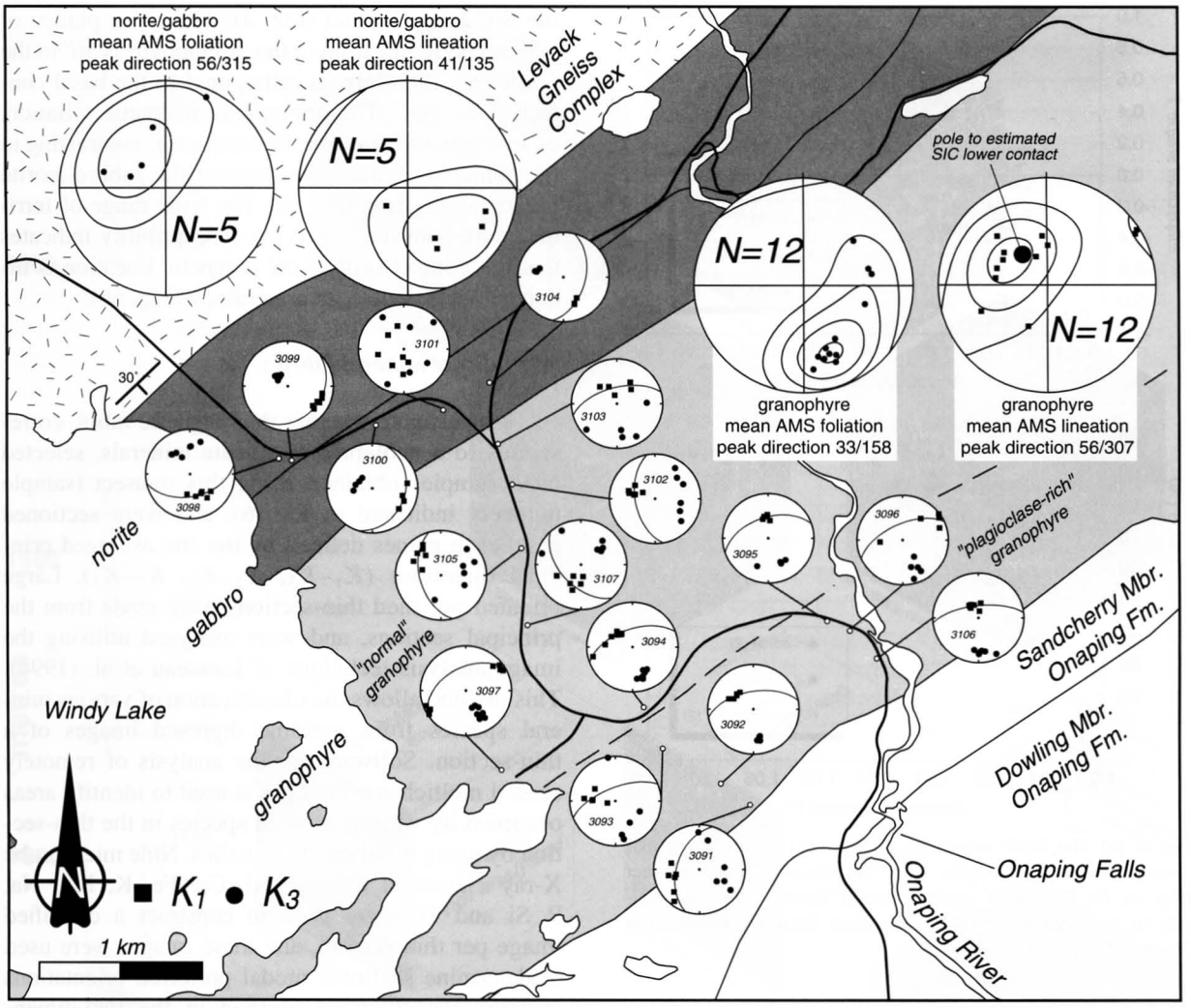

Fig. 4. AMS data from the Onaping Falls transect (Fig. 1; domain *A* of Fig. 8). Individual stereoplots from each site show the scatter in individual cylinder measurements. Mean magnetic foliations for each site are indicated as a great circle, with the exception of 3101 where there is too much scatter in the data for accurate determination of the foliation orientation. The dip of the SIC basal contact is dipping ~30° SE (Naldrett and Hewins, 1984). Stratigraphic subdivision of the Onaping Formation into Sandcherry and Dowling Members is after Ames and Gibson (1995).

bro and norite units, respectively, along this transect (Fig. 4). Four to seven cylindrical specimens (2.2 cm long and 2.54 cm in diameter) were extracted by drilling from each oriented block. The AMS principal axes and parameters P', T were determined for each core sample and site averages were calculated. The percentage of K_{ferri} was also determined using the empirical relationship shown graphically in Fig. 2 (Fig. 5).

The AMS fabrics of the SIC lithologies along this transect indicate that the gabbro and norite units exhibit very similar orientations of AMS principal axes. Gabbro–norite is characterised by contact-parallel magnetic foliation (34° SE dip) and down-dip oriented magnetic lineation as indicated by the individual and site-averaged stereoplots (Fig. 4). The base of the SIC in this area is known to be dipping ca. 30° to the southeast (Rousell, 1984, fig. 5.1),

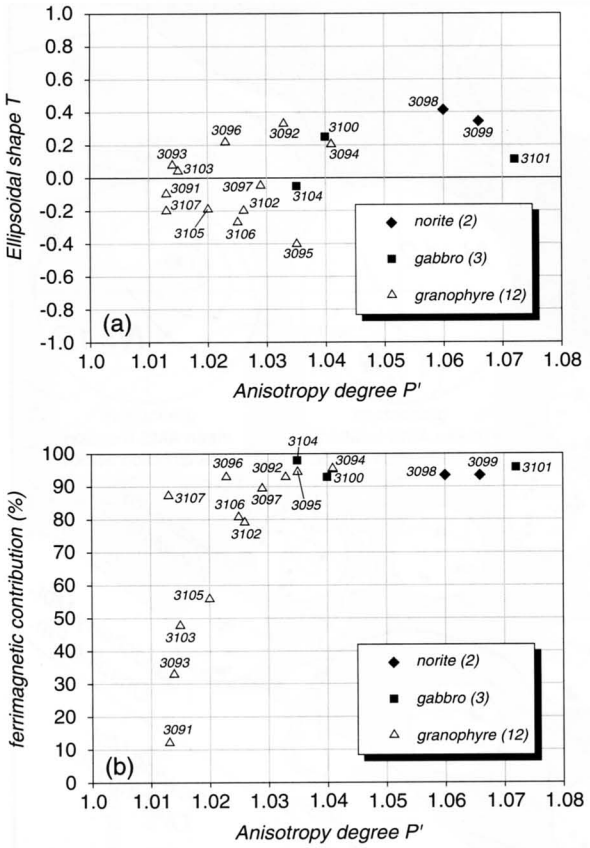

Fig. 5. (a) The AMS anisotropy degree (P') versus ellipsoidal shape (T) for the samples from the Onaping Falls transect (Fig. 4). (b) Plot of P' against percent ferrimagnetic contribution to low-field susceptibility obtained from the relationship illustrated in Fig. 2.

hence the magnetic foliation is subparallel to this contact. The regional pattern of gabbro–norite igneous fabric is subparallel to the basal contact of the SIC, and the lineation radial with respect to the ovoid Sudbury Basin (Cowan, 1996; Cowan et al., 1999).

The magnetic fabric of the granophyre, in contrast, is distinctly different from that of the gabbro–norite. The orientation of the magnetic lineation is well-defined and is orthogonal to the orientation of the SIC basal contact (Fig. 4). The mean plunge of the magnetic lineation in the granophyre is 56° to the northwest, therefore, is orthogonal to the basal contact of the SIC. The granophyre magnetic foliation, on average, dips toward the northwest, contrasting to the contact-parallel orientation of the gabbro–norite magnetic foliation (Fig. 4). The wide range of ferrimagnetic contribution to the susceptibility indicates that the contact-orthogonal magnetic lineation is independent of magnetic mineralogy (Fig. 5b).

3.2. Silicate mineral fabrics

To investigate whether the magnetic fabric corresponds to a subfabric of silicate minerals, selected hand samples obtained along this transect (sample numbers indicated in Fig. 6), and were sectioned parallel to planes defined by the site averaged principal directions (K_1–K_3, K_1–K_2, K_2–K_3). Large oriented polished thin-sections were made from the principal sections, and were analysed utilising the image analysis technique of Launeau et al. (1994). This method allows the identification of various mineral species from multiple digitised images of a thin-section. Software for the analysis of remotely sensed multichannel images is used to identify areas occupied by various mineral species in the thin-section by using multivariate statistics. Nine microprobe X-ray elemental images (Al, Ca, Fe, K, Mg, Na, P, Si and Ti) were used to construct a classified image per thin-section, and these images were used to determine sectional modal preferred orientations utilising the *Intercept Method* in the two-dimensional faces (Launeau and Robin, 1996). Several mineral modes were identified in each thin-section (plagioclase, quartz, K-feldspar, albite, amphibole, opx, cpx, apatite, biotite, magnetite, and alteration products of magnetite), but most minerals were combined for the purpose of fabric analysis (see Cowan, 1996, for detailed description of the microprobe procedure). A graphical representation of the analysed rock faces is illustrated in Fig. 6 as three-dimen-

Fig. 6. The plagioclase fabrics of the plagioclase-rich granophyre, normal granophyre, and the norite from some of the AMS samples. The stratigraphic section of the SIC is in true thickness, assuming 30° dip at the Onaping Falls transect. Block diagrams are drawn with respect to the SIC contact-normal direction (vertical in this plot, i.e., parallel to K_1 and K_3 in the granophyre, and norite samples respectively).

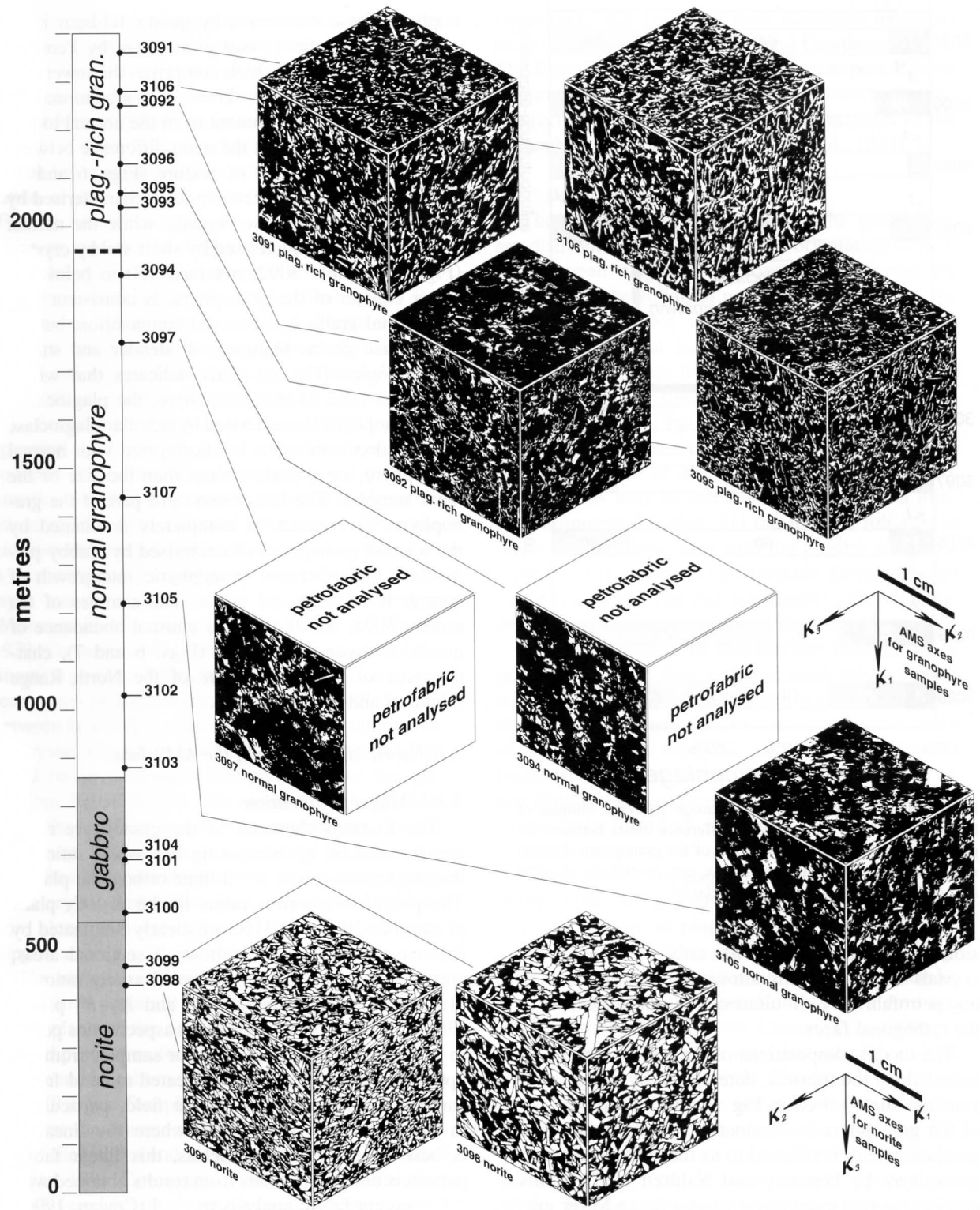
plag.-rich gran.
normal granophyre
gabbro
norite
metres
2000
1500
1000
500
0
3091
3106
3092
3096
3095
3093
3094
3097
3107
3105
3102
3103
3104
3101
3100
3099
3098
3091 plag. rich granophyre
3106 plag. rich granophyre
3092 plag. rich granophyre
3095 plag. rich granophyre
petrofabric not analysed
petrofabric not analysed
3097 normal granophyre
petrofabric not analysed
petrofabric not analysed
3094 normal granophyre
1 cm
K3
K2
K1
AMS axes for granophyre samples
3105 normal granophyre
3099 norite
3098 norite
1 cm
K2
K1
K3
AMS axes for norite samples

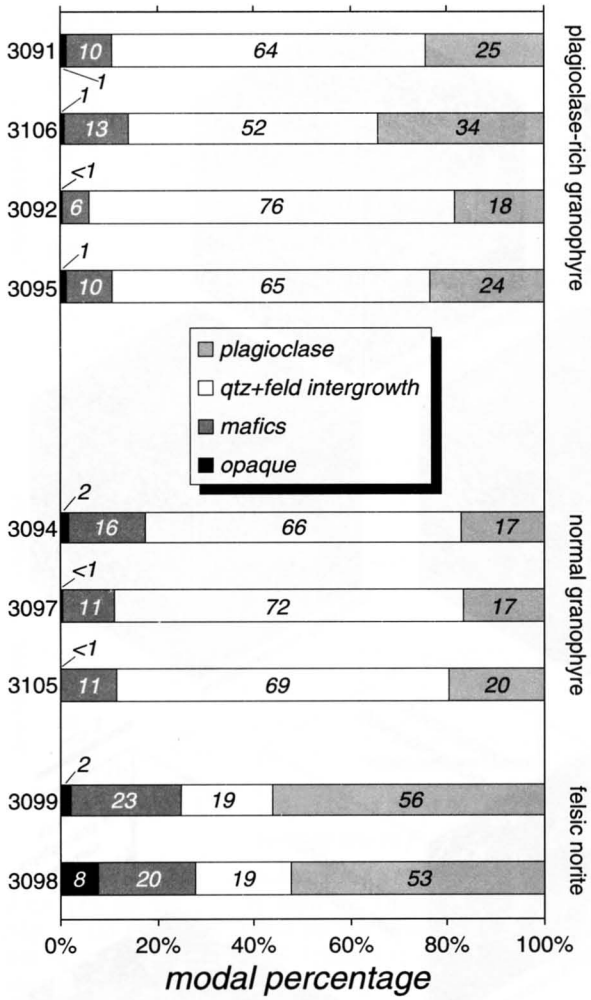

Fig. 7. Modal compositions of the image analysed samples of Fig. 6. Only small compositional difference exists between the plagioclase-rich and normal varieties of the granophyre. Various mafic minerals in the felsic norite (opx, cpx, amphibole, chlorite) are not differentiated for the sake of clarity.

sional block diagrams, with only the plagioclase crystals displayed. This allows the identification of any petrofabric by simultaneous visual inspection of the orthogonal faces.

The modal compositions of the rock samples collected along the transect, determined by image analysis, are summarised in Fig. 7. The uppermost 1/3 of the granophyre is dominated by an acicular plagioclase, which is referred to as the *plagioclase-rich granophyre* by Peredery and Naldrett (1975). This plagioclase-rich granophyre grades into a lower granophyre phase dominated by quartz–feldspar intergrowths called the *normal granophyre* by Peredery and Naldrett (1975) which comprises the lowermost 2/3 of the granophyre. There is a gradational increase in plagioclase content from the normal to plagioclase-rich phase, but the main difference between the two phases is that of texture (Figs. 6 and 7). The plagioclase-rich granophyre is characterised by long slender plagioclase crystals, while the normal granophyre, is characterised by short stubby crystals (Fig. 6). Sample 3092, obtained 150 m below the upper contact of the granophyre, is consistent with the normal granophyric modal composition, but the plagioclase grains feature both slender and stubby morphologies (Fig. 6). This indicates that within the upper third of the granophyre, the plagioclase-rich granophyre characterised by acicular plagioclase crystals dominates, but is interlayered with normal granophyre, on a scale greater than the size of the hand samples. The lower two-third part of the granophyre, in contrast, is completely dominated by the normal granophyre characterised by stubby plagioclase and abundant granophyric intergrowth of quartz, K-feldspar and albite. The samples of the norite (3098, 3099) show an unusual abundance of quartz–feldspar intergrowth (Figs. 6 and 7), characteristic of the *felsic norite* of the North Range (Naldrett and Hewins, 1984).

3.3. Fabric significance of the AMS data

3.3.1. Magnetic lineation

The lineated character of the granophyre rocks can be realised by comparing the aspect ratios of the plagioclase grains in all three orthogonal planes. The plagioclase aspect ratios in the K_2–K_3 plane of samples 3095 and 3106 are clearly dominated by low-aspect-ratio grains with small sectional areas, compared to the elongate sectional aspect ratios of plagioclase seen in the K_1–K_3 and K_1–K_2 planes (Fig. 6). This pattern of sectional aspect ratios points to a mineral lineation, at least for samples from the uppermost granophyre. This lineated mineral fabric can readily be identified in the field, particularly in the uppermost granophyre where the lineation is best developed. Nevertheless, this linear fabric pattern is not conspicuous from results obtained with the intercept fabric analysis method (Cowan, 1996).

This may be related to the low anisotropy of the granophyre fabric, and the fact that the lineation can be detected by eye when defined by a few slender plagioclase crystals (e.g., mineral lineation in sample 3095 is defined by several slender plagioclase crystals in the K_1–K_3 and K_1–K_2 planes; Fig. 6).

The widespread contact-orthogonal magnetic lineation in the lower two-thirds of the granophyre (Fig. 4) has no counterpart in the visible shape fabric of the silicate minerals (Fig. 6). This could be explained by a lower degree of mineral fabric anisotropy at the scale of a single thin-section. Regardless of the absence of strong silicate mineral lineation in the normal granophyre, the contact-orthogonal magnetic lineation is interpreted to be the result of igneous crystallisation. Since the magnetic lineation correlates to a mineral lineation in the uppermost granophyre, it is reasonable to expect a common origin for the contact-orthogonal magnetic lineation found throughout the granophyre along this transect. The contact-normal orientation of the plagioclase and amphibole (altered pyroxenes) crystals is explicable as part of a crescumulate or comb-layer texture described from intrusions elsewhere (Moore and Lockwood, 1973; McBirney and Noyes, 1979; Carpenter, 1983). Subordinate contact-parallel lineation patterns (3096, 3097) are interpreted to represent sites of contact-parallel crystal growth formed between layers of contact-orthogonal crystal growth.

Crystal alignment resulting from magmatic flow could be an alternative interpretation for the granophyre lineation, but this mechanism is unlikely since the acicular plagioclase morphology of the uppermost granophyre is not likely to have survived flow-induced rotations and collisions in a magmatic crystal slush. The contact-orthogonal orientation, along with the delicate crystal morphologies, support an origin due to in-situ crystal growth.

The magnetic lineation of the felsic norite correlates to a preferred orientation of mineral grains in the plane of the igneous foliation (Fig. 6). This down-dip lineation found along this transect is similarly found in gabbro–norite samples in the East and South Ranges. Samples from around the SIC indicate that the lineation–foliation (L–S) igneous fabrics of the gabbro and norite are essentially identical (Cowan, 1996; Cowan et al., 1999). Mineral lineation from layered igneous rocks have not been reported extensively, but few have been described nevertheless (Nicolas, 1992; Quadling and Cawthorn, 1994). The lineation fabric of the norite is interpreted to be the product of magmatic flow, in contrast to the exclusively growth-controlled mineral lineation of the granophyre (Cowan, 1996; Cowan et al., 1999).

3.3.2. Magnetic foliation

The magnetic foliation poles of the granophyre are distributed in a partial girdle orientation normal to the mean magnetic lineation (Fig. 3), with the majority of the foliation poles plunging toward the south-southeast. No subfabric of silicate minerals seem to exist that can be correlated to the magnetic foliation (Fig. 6). In fact, for sample 3106, a weak plagioclase lineation is subparallel to K_3 in the K_2–K_3 plane, but K_3 should be normal to the alignment of silicate minerals in this plane (Fig. 6; see also Cowan et al., 1999, fig. 3d). Alternative explanations may be offered for the lack of a mineral alignment foliation: (1) the mineral foliation is weak and not detectable with the present analytical methods; (2) a superposed tectonic fabric affected the AMS fabric, but did not significantly alter the original crystallisation fabric of the granophyre.

It is not possible to differentiate between these possibilities from data gathered from this sampling transect. It is significant to point out, however, that there is no evidence for pervasive solid-state strain of the granophyre along this transect. Isolated brittle faults have been observed, but the quartz grains do not display extensive undulose extinction indicative of subgrain boundary formation due to solid-state deformation.

The magnetic foliation of the norite samples correlates with an igneous foliation defined by preferred alignment of plagioclase and pyroxene crystals (Fig. 6). The contact-parallel nature of this igneous foliation is found in norite and gabbro samples around the Sudbury Igneous Complex (Naldrett and Hewins, 1984; Cowan, 1996; Cowan et al., 1999).

In summary, the norite magnetic fabric correlates with a triaxial mineral fabric. The igneous foliation of the norite is subparallel to the basal contact of the SIC, and the mineral lineation is oriented down-dip. Compared to the gabbro–norite fabric, the silicate fabric of granophyre, is approximately a pure linear fabric. The magnetic lineation is consistent through-

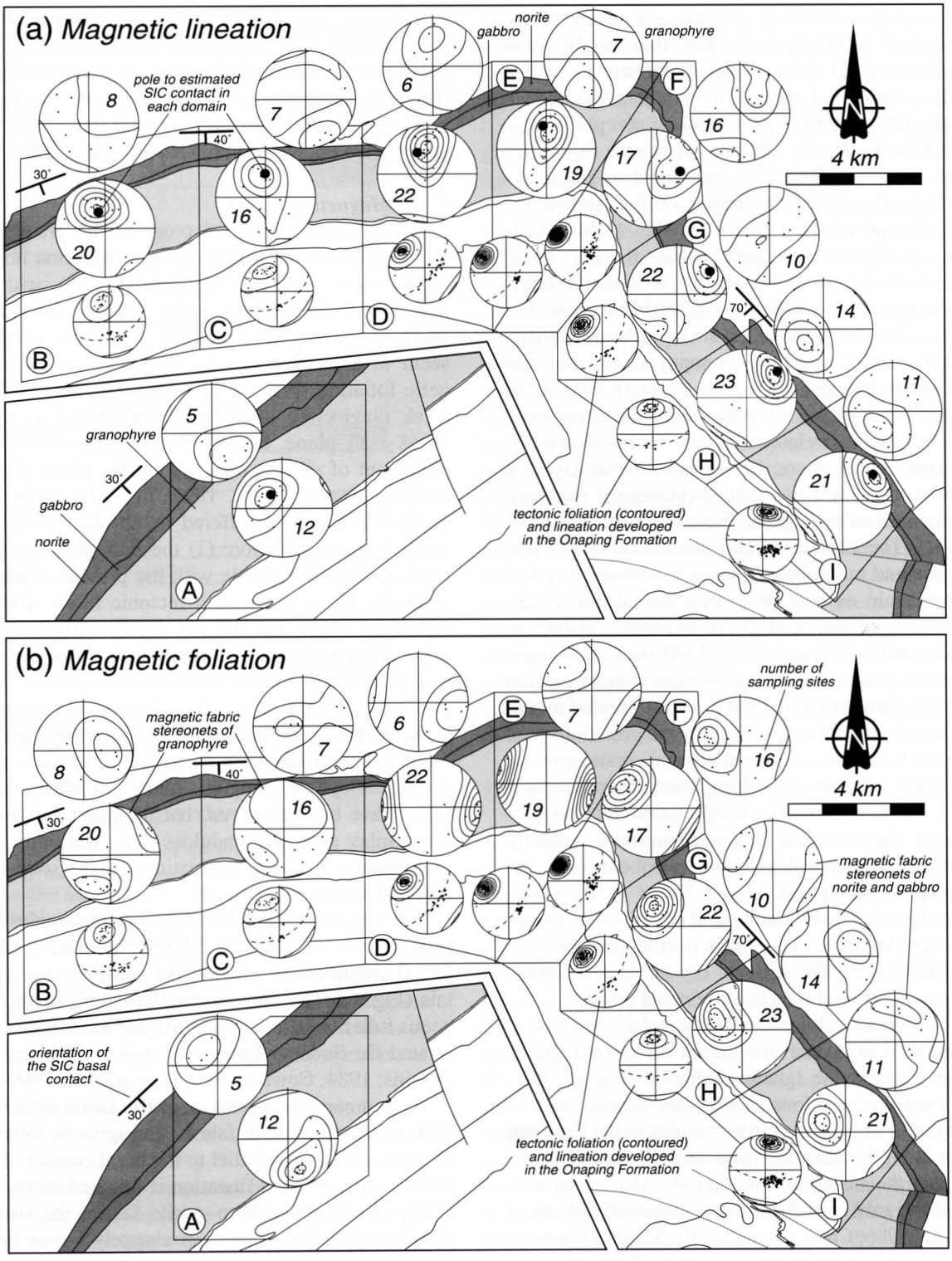
(a) Magnetic lineation
norite
gabbro
granophyre
pole to estimated SIC contact in each domain
40°
30°
4 km
tectonic foliation (contoured) and lineation developed in the Onaping Formation
(b) Magnetic foliation
number of sampling sites
magnetic fabric stereonets of granophyre
magnetic fabric stereonets of norite and gabbro
orientation of the SIC basal contact
70°
A
B
C
D
E
F
G
H
I

out the granophyre, and is orthogonal to the SIC contact boundary. Where this magnetic lineation can be correlated to a silicate fabric, it is defined by aligned acicular crystals of plagioclase and amphibole, consistent with crescumulate or comb-layering texture described from intrusions elsewhere. While a magnetic foliation can be detected in the granophyre, it cannot be correlated to a visible silicate foliation in the granophyre.

Recognition of the granophyre to be a lineated rock (Figs. 4 and 6), together with the information that the magnetic fabric orientations are independent of magnetic mineralogy (Figs. 3 and 5b) are significant features that will aid in estimating strains of the eastern SIC. Comparisons of the Onaping Falls transect are made below with the AMS data obtained from the northeastern quadrant of the Sudbury Igneous Complex.

4. Magnetic fabrics of the East and North Ranges

4.1. Magnetic fabric patterns of the gabbro–norite and granophyre

The AMS data obtained from the eastern SIC in the East and North Ranges are summarised in Figs. 8–11. Contoured, equal-area stereoplots of magnetic foliation and lineations of the granophyre and gabbro–norite are shown for domains *B* to *I*, along with domain *A* which is the Onaping Falls transect described above (Fig. 8). A total of 84 and 172 AMS sites are represented for the gabbro–norite, and granophyre sample localities, respectively, and for each site an average of six cylindrical samples (total of more than 1400 cylinder samples) were used to obtain the mean AMS fabrics displayed in Figs. 8 and 9. Tectonic schistosity and lineation measurements from the adjacent Onaping Formation are summarised for comparison for each domain, with the exception of domain *A* where there is no macroscopic deformation (Fig. 8). Susceptibility (K), percentage ferrimagnetic susceptibility (K_{ferri}), and modified anisotropy degree (P'), shapes of magnetic ellipsoids (T) are summarised in Figs. 10 and 11, respectively. All raw AMS data for both single cylinder and site averages for all samples obtained in this study are summarised in Cowan (1996).

The magnetic fabrics similar to those of the Onaping Falls transect (domain *A*) are identifiable in both the granophyre and gabbro–norite phases. The magnetic fabric of the gabbro–norite, which conforms with the contact-parallel foliation and down-dip lineation, is best seen in domains *H* and *I* (Figs. 8 and 9). Elsewhere this pattern is not clear, perhaps due to the very low susceptibility values in the specimens collected from the North Range (domains *B*, *C* and *D*; Fig. 10). In domain *E* the magnetic lineation of the gabbro–norite plunges to the south as expected, but the magnetic foliation is not contact-parallel but appears to be axial-planar to the fold-like juncture between the North and East Ranges (henceforth referred to as the *North Lobe*). A similar axial-planar magnetic foliation is seen in the gabbro–norites of domains *F* and *G*.

The magnetic fabrics of the granophyre are more clearly defined than those of the gabbro–norite (Fig. 8). The most pronounced feature of the granophyre AMS is its well-defined magnetic lineation (Fig. 8a and Fig. 9a). The site mean of granophyre magnetic lineation is generally contact-orthogonal, as far as it can be determined from published dip values of the base of the SIC in the East and North Ranges (Rousell, 1984, fig. 5.1; Cowan et al., 1999, fig. 5; compare contoured magnetic lineation peaks with approximate poles to SIC contacts at each domain in Fig. 8a). The contact of the SIC in the North Range dips 30°–40° to the south, and the magnetic lineations in domains *B*, *C*, *D* and *E* plunge ca. 40°–55° to the north. Similarly, the East Range granophyre lineations plunge ca. 25° to the northeast where the SIC contact is know to be dipping 60°–

Fig. 8. Stereoplots of (a) site mean magnetic lineation, and (b) site mean magnetic foliation measurements for the study areas (Fig. 1). Stereoplots are divided into domains *A* to *I*. Numbers of station means shown in the stereonets. Measurements of tectonic foliation from the adjacent Onaping Formation (contoured) and lineation (not contoured) are shown (contour method of Robin and Jowett, 1986). Mean tectonic foliation is drawn as a dashed great circle in the Onaping plots. Dips of the North and East Ranges from Rousell (1984), and their approximate poles are indicated on the stereoplots of the granophyre magnetic lineation in (a). Note the parallelism between these poles (in black circles) in each domain and the contour peaks of the magnetic lineations in the granophyre.

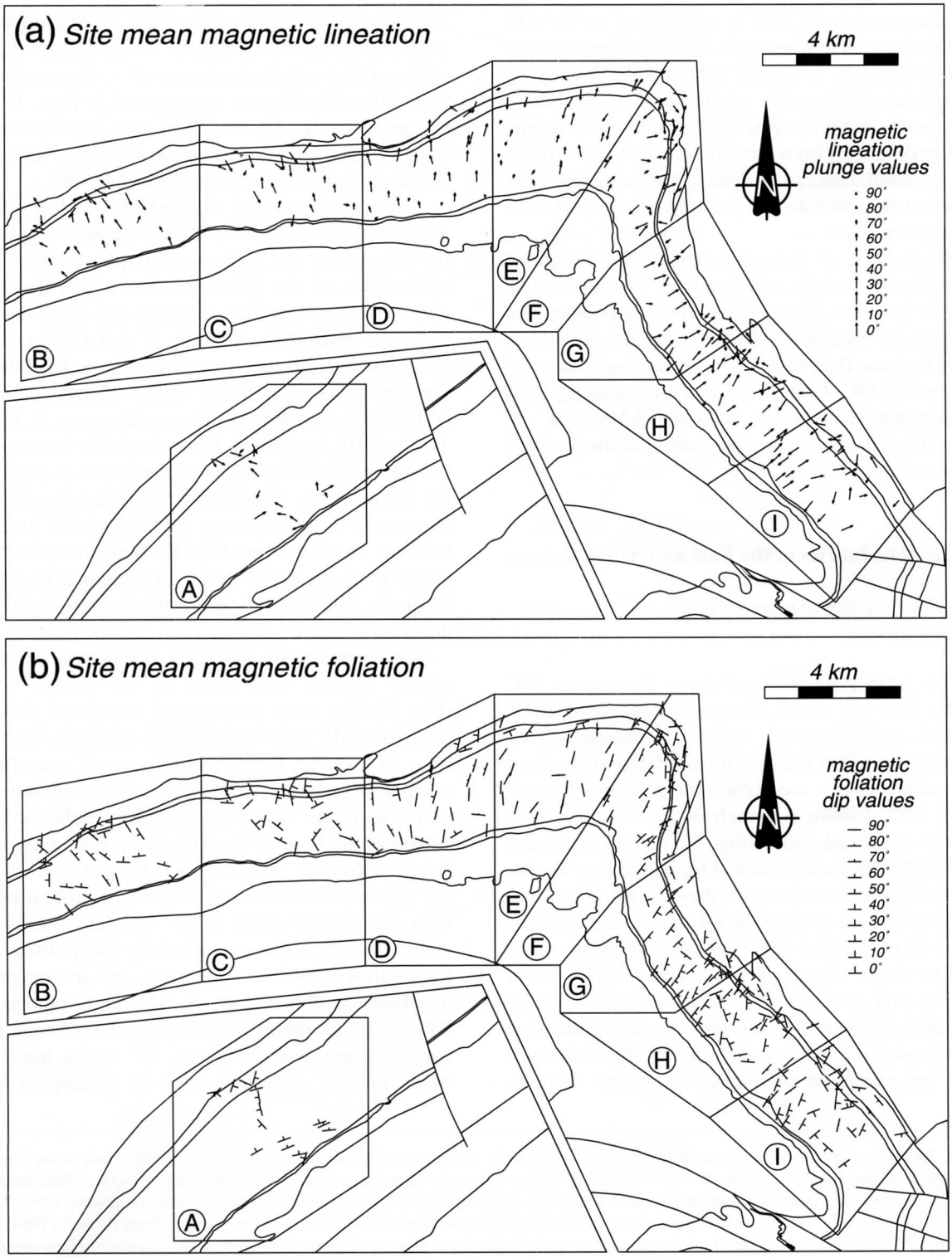

Fig. 9. (a) Site mean magnetic lineation, and (b) site mean magnetic foliation measurements for the study areas (Fig. 1). Sample stations located at the base of lineation arrow and centre of dip symbols.

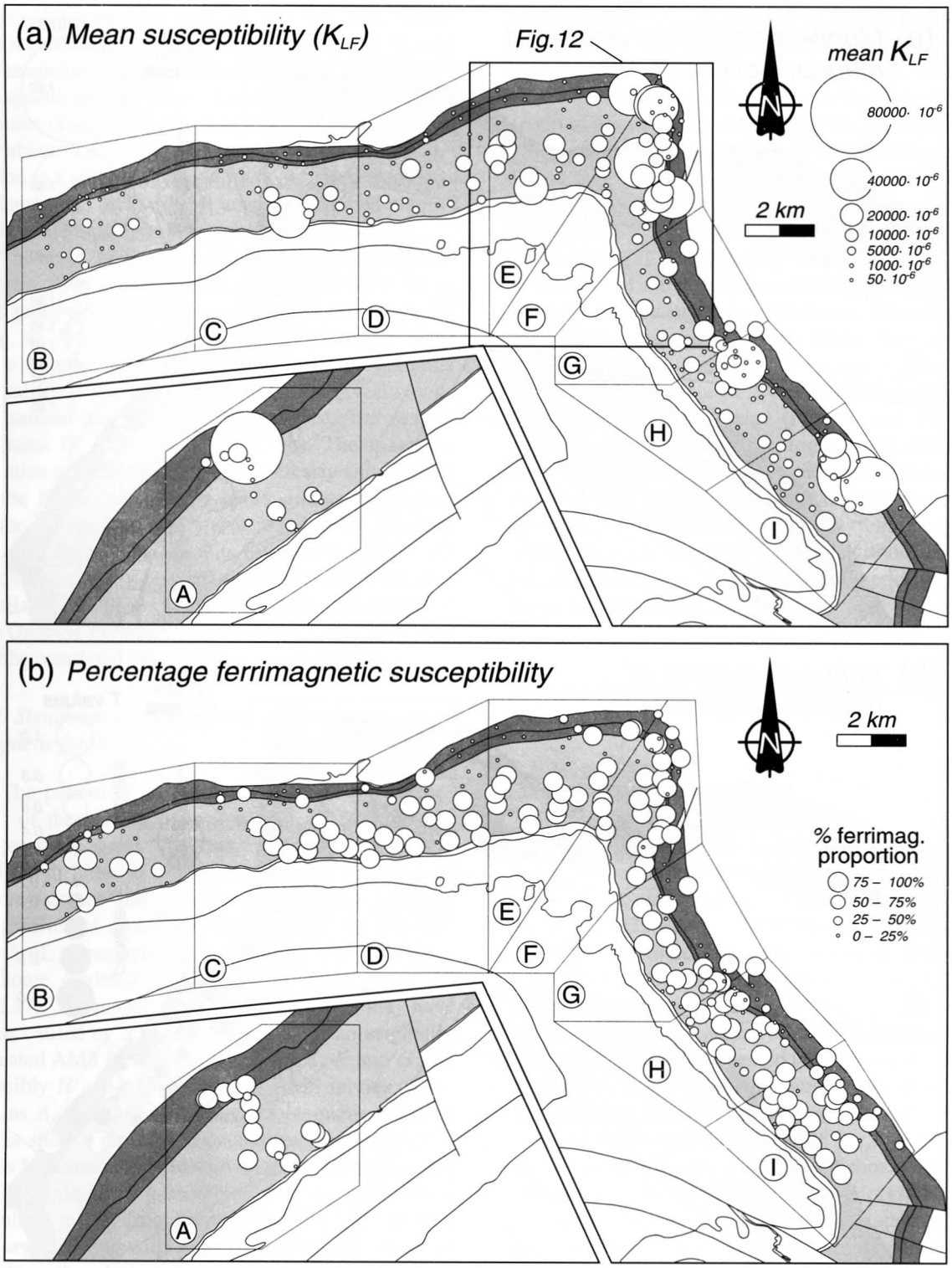

Fig. 10. (a) Mean low field susceptibility K_{LF}, and (b) proportion of ferrimagnetic susceptibility K_{ferri} calculated from the relationship in Fig. 2 for each site.

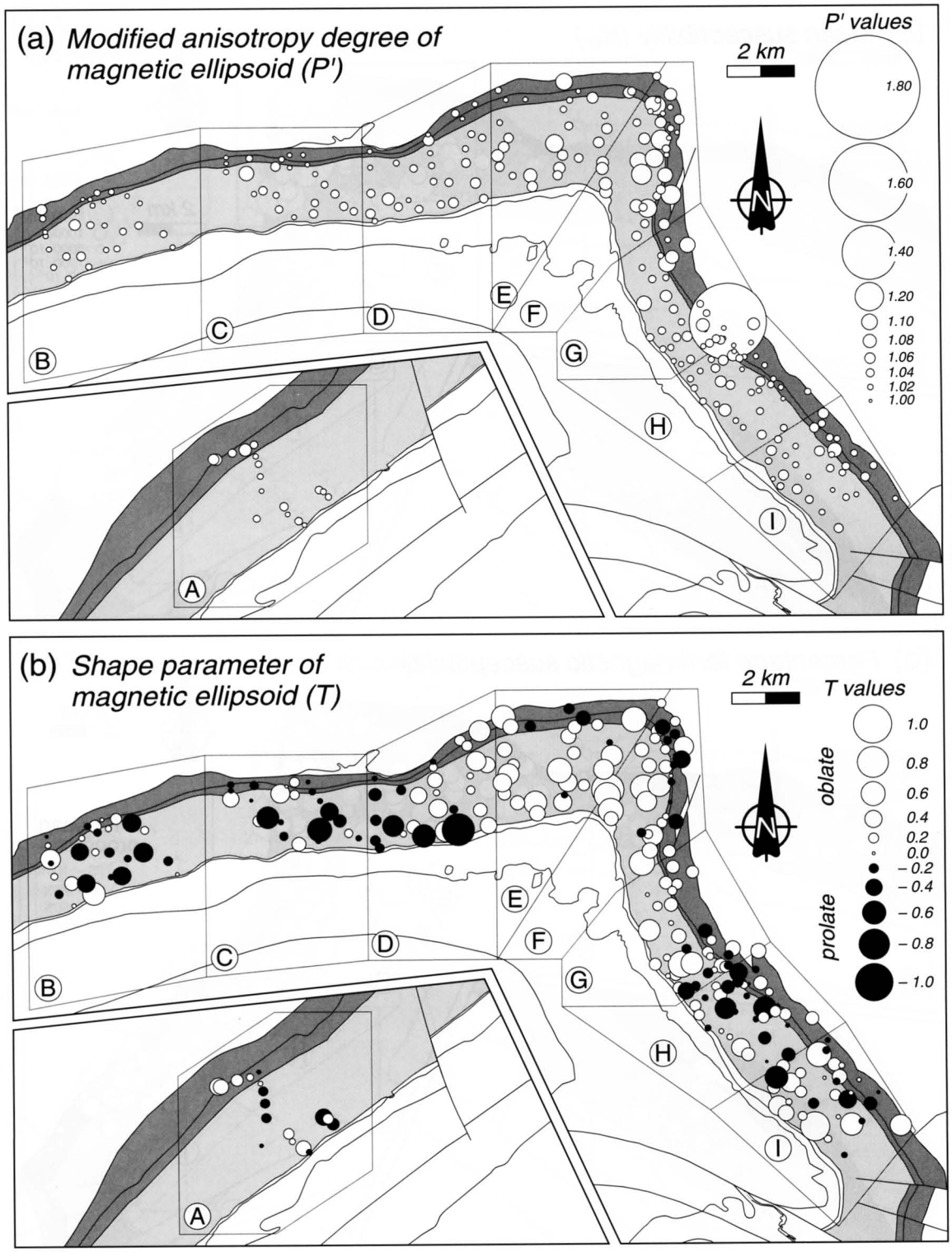

Fig. 11. (a) Mean AMS modified anisotropy degree P', and (b) shape parameter T, for each site.

70° to the southwest (Fig. 8a and Fig. 9a). These contact-orthogonal relationships (Figs. 8 and 9), and the magnetic lineation defined by wide ranging ferrimagnetic content (Figs. 3 and 10) are identical to features observed in the domain *A* discussed in detail above. The correspondence of this magnetic lineation to a silicate lineation was confirmed by visual examination of sawed and chemically stained plagioclase-rich granophyre samples of the East Range.

The magnetic foliation poles of the granophyre of domain *A* lie along a great-circle with most foliation poles plunging shallowly to the south-southeast (Fig. 4). A similar great-circle distribution of magnetic foliation poles characterise those of domains *B* and *C*. This great-circle distribution gives way to a clustered distribution further towards the east in domains *D*, *E*, *F* and *G* (Fig. 8b). The magnetic foliation of these four domains is clearly axial-planar to the North Lobe, and exhibit similar orientation as the tectonic schistosity developed in the adjacent Onaping Formation (Fig. 12). Further, magnetic foliation of the granophyre in domains *H* and *I* are also similar to the axial-planar schistosity orientation of the Onaping Formation in the North Lobe, but could not be correlated with a visible mineral fabric.

4.2. Significance of the regional granophyre magnetic fabrics

The pattern of magnetic foliation in the eastern half of the SIC suggests a spatial relationship between the magnetic foliation of the granophyre and the North Lobe. It is evident from the presence of microfractures and presence of prismatic subgrain boundaries of quartz (cf. Kruhl, 1996) in thin-sections of granophyre in the North Lobe that there is some evidence for solid-state strain (Figs. 12 and 13). The magnetic foliation, therefore, may have been caused by a tectonic overprint of an originally lineated AMS fabric in domains *D*, *E*, *F* and *G* and possibly *H* and *I* (Fig. 8b). The AMS fabrics of domains *A*, *B* and *C* reveal that the magnetic foliation poles show a girdle > cluster distribution (Fig. 8b). This foliation pattern resembles the original lineated AMS fabric of the granophyre, with the AMS fabric resulting mostly from the contact-orthogonal growth of crystals, but with a weak superposed strain to produce the cluster of foliation poles. The cluster strength of the foliation poles (Fig. 14), as well as the oblateness of AMS ellipsoids (*T* values; Fig. 11b), increases as the North Lobe is approached. Both evidence is consistent with a tectonic overprint for the origin of the magnetic foliation of the granophyre.

Nevertheless, the question of whether the degree of deformation seen in the North Lobe (domains *E* and *F*) is consistent with the folding of an originally horizontal SIC cannot be adequately addressed by microstructural examinations alone (Fig. 13). The strain level of the granophyre, however, can be modelled from the measured AMS fabric, assuming that the original granophyre AMS fabric was initially lineated prior to the tectonic overprint. The contact-orthogonal magnetic lineation of the granophyre is recorded in all domains (Fig. 8a and Fig. 9a); therefore, the cumulative tectonic strain could not have exceeded a level that would have substantially modified this AMS fabric. A numerical method of estimating the degree of tectonic shortening required to produce the weak AMS foliation, without substantial modification to the original magnetic lineation, is examined below.

5. Numerical modelling of granophyre AMS patterns

5.1. Methodology

5.1.1. Initial pure lineation fabric

The AMS of a rock is the function of the intrinsic susceptibility anisotropies of the individual particles (P_c) and their orientations (Owens, 1974; Richter, 1992; Benn, 1994). The numerical simulation is simplified when the magnetic grains are considered as prolate ellipsoids of revolution with particle susceptibilities of $k_a \geq k_b = k_c$ and the intrinsic susceptibility anisotropy P_c is given by k_a/k_c. A hypothetical rock dispersed with magnetite, for example, can be modelled by using ranges of intrinsic susceptibility anisotropies of magnetite ($P_c = 1.18$ according to Borradaile et al., 1987, 1.3–1.5 according to Archanjo et al., 1995 and Rochette, 1994a,b), and assign orientations to individual crystals. Once the individual crystals are oriented appropriately, the susceptibility tensors for individual particles are summed and the whole-rock AMS calculated. The

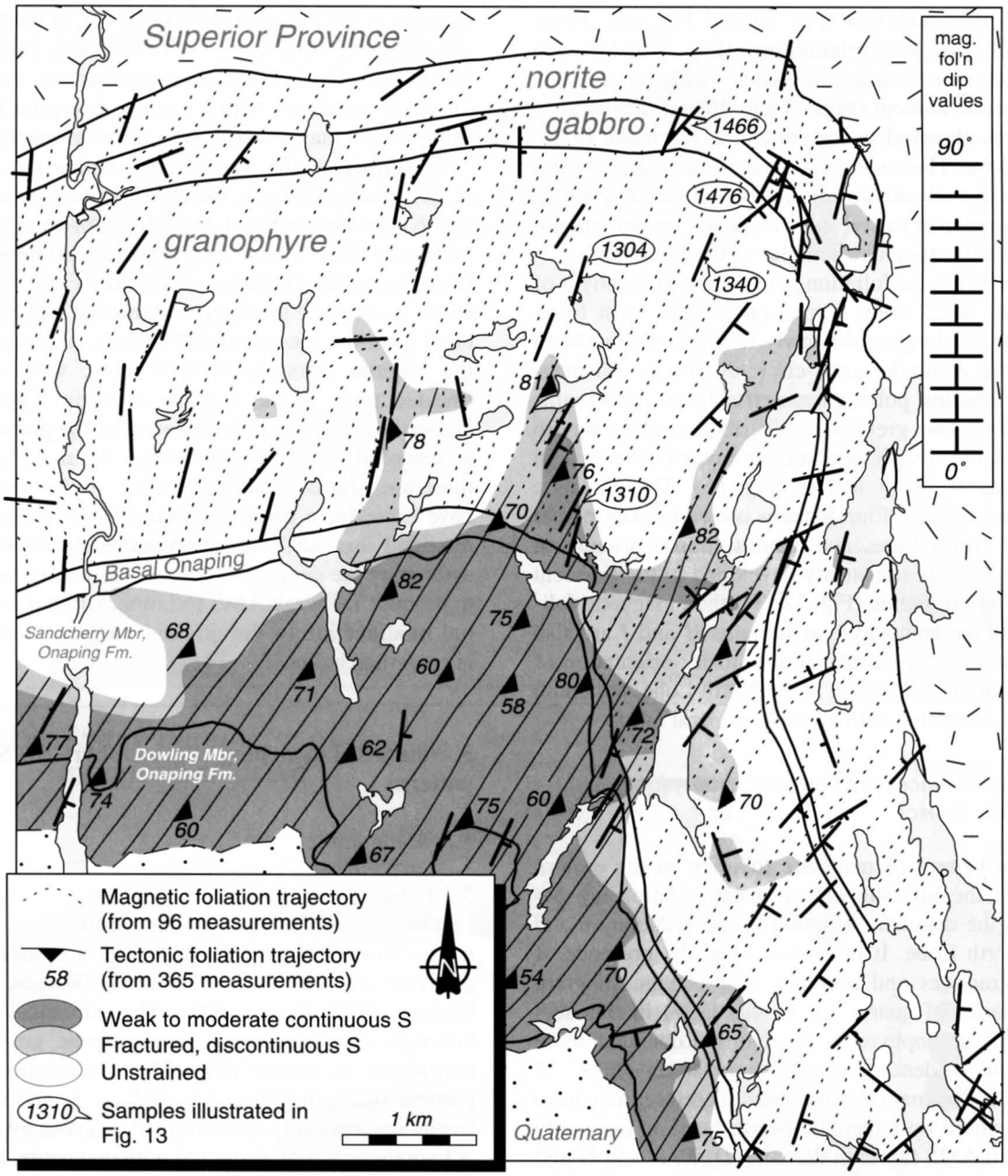

Fig. 12. Map of magnetic foliation trajectories of the SIC, and tectonic schistosity trajectories of the SIC and the Onaping Formation in the North Lobe (location shown in Fig. 10a). The solid trajectories were constructed from the tectonic foliation of the Onaping Formation and the uppermost granophyre. The dashed trajectories are constructed from site mean magnetic foliations from the SIC (all magnetic foliation measurements used to construct the trajectory field are shown). Both trajectory systems were constructed with a computer program that performs objective interpolation of trajectories (Cowan, 1996). Note a zone of solid-state strain (as indicated by shading) along a NNE-trending fault zone marked by a linear arrangement of lakes on the east limb of the North Lobe. The rocks along this zone are cataclastically deformed, but elsewhere in the North Lobe the strain is low to absent (see Fig. 13).

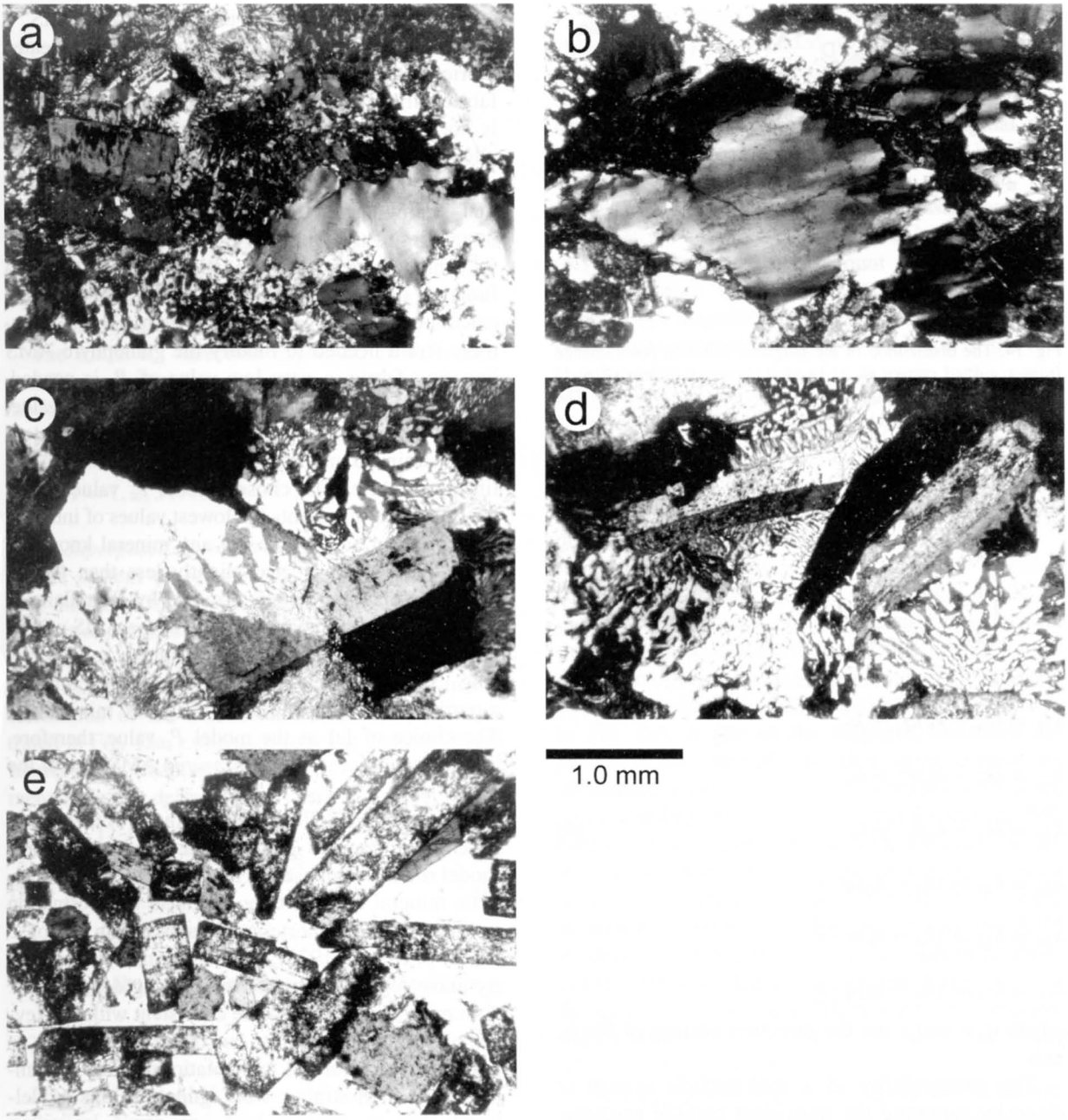

Fig. 13. Photomicrographs (a) to (e) are of samples obtained from the hinge region of the North Lobe, with (a) being a granophyre sample obtained closest to the Onaping contact, and (e) a gabbro sample, closest to the outer arc (see Fig. 12 for localities). Samples from the hinge of the North Lobe are illustrated because this area would exhibit the highest solid-state strains if the SIC was folded from a consolidated horizontal sheet. Granophyre sample 1310 of (a) exhibits the highest strain in this area of the North Lobe, featuring microfractures and undulose extinction of quartz. The plagioclase is still angular, and bulk strain is consistent with minor shortening. Samples 1304, 1340 and 1476 (b, c, and d) exhibit restricted undulose extinction in quartz, and all appear macroscopically undeformed in the field (Fig. 12). The strain level is not severe as crystal outlines of plagioclase grains can be deciphered in samples 1340 (c) and 1476 (d). Also preserved are the delicate quartz–feldspar intergrowths, attesting to the very low strains. The gabbro sample 1466 (e) exhibits no sign of quartz deformation. While the plagioclase is extensively saussuritised in this sample, the euhedral outlines of the plagioclase are clearly preserved, indicating no solid-state strain.

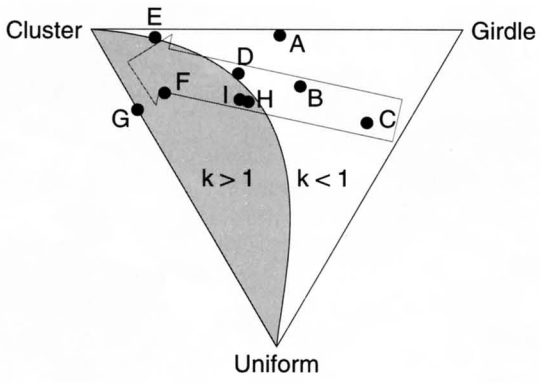

Fig. 14. The distribution of the magnetic foliation poles change from a girdled pattern ($k < 1$) to a clustered pattern ($k > 1$) as the North Lobe is approached (direction of the arrow). The ternary plot represents cluster, girdle and uniform distributions at each of its apex (Vollmer, 1990).

individual grain susceptibility tensor is given by:

$$\mathbf{k}_{ij} = \begin{pmatrix} k_{11} & k_{12} & k_{13} \\ k_{21} & k_{22} & k_{23} \\ k_{31} & k_{32} & k_{33} \end{pmatrix} \tag{3}$$

where $\mathbf{k}_{ij}$ is a symmetric tensor and:

$$k_{11} = (k_a - k_b)q^2 + k_b$$

$$k_{22} = (k_a - k_b)r^2 + k_b$$

$$k_{33} = (k_a - k_b)s^2 + k_b \tag{4}$$

$$k_{12} = k_{21} = (k_a - k_b)q \cdot r$$

$$k_{23} = k_{32} = (k_a - k_b)r \cdot s$$

$$k_{13} = k_{31} = (k_a - k_b)q \cdot s$$

where q, r and s are the direction cosines of the k_a axis.

The susceptibility of a multiparticle system is given by summing the individual particle susceptibility tensors and determining the eigenvalues. The orientation of the AMS ellipsoid is given by the eigenvectors of the total susceptibility tensor $\mathbf{K}_{ij}$:

$$\mathbf{K}_{ij} = \frac{1}{n} \sum_{n}^{m=1} (k_{ij})_m \tag{5}$$

where n is the total number of magnetic particles.

For the simulation of the granophyre AMS, a fabric must be first created to represent the lineated fabric of the granophyre prior to deformation. This fabric, since it results from preferred crystal growth, is not a strain fabric, but can be nevertheless modelled as a consequence of strain, termed herein as *virtual strain* (cf. Robin, 1977). The required virtual strain needed to simulate the AMS ellipsoid intensities of the Onaping Falls transect (Figs. 4 and 5), which have an average P' value of 1.024, is a function of the chosen model P_c value. In order to calculate a conservative upper limit value of tectonic strain needed to modify the granophyre AMS lineation fabric, a very low value of P_c is needed, since this would require a large virtual strain value, which in turn must be overcome by a large tectonic strain to modify the original igneous AMS lineation fabric. The chosen model P_c value is 1.1, for this value represents the lowest values of intrinsic susceptibility anisotropies of any mineral known to cause AMS, and is also slightly less than the P_c value for magnetite as determined by Borradaile et al. (1987). Since the orientations of the AMS principal axes are independent of the magnetic mineralogy (Fig. 3), the model P_c value is not constrained to a particular value specified by magnetic mineralogy. The choice of 1.1 as the model P_c value, therefore, does not conflict with the measured AMS data of the SIC.

The AMS modelling assumes that: (1) there is an absence of grain to grain magnetic interaction; (2) model rock is composed of monomineralic bulk magnetic mineral composition; (3) linear transformation is used to model shortening strains (strain response model of March, 1932); and (4) intrinsic susceptibility anisotropy remains constant during deformation. Assumptions (3) and (4) are consistent with low levels of shortening strains, but other factors such as grain shape distortion and rotations which are important at high strains, were ignored in this modelling.

The following steps are used for the modelling.

A computer random number function is used to generate randomly oriented k_a directions for 500 particles ($n = 500$). To create the initial igneous comb-layer fabric of the granophyre the following constrictional deformation matrix is used (virtual strain):

$$\mathbf{D}_v = \begin{pmatrix} \frac{1}{S_v} & 0 & 0 \\ 0 & S_v & 0 \\ 0 & 0 & S_v \end{pmatrix} \quad (6)$$

where S_v is the axial shortening value assigned to produce the prolate AMS fabric. The P' value of the granophyre is a function of both S_v and P_c values. It was found from trial and error that a S_v value of 0.75 (25% constriction) resulted in a suitable P' value representative of the granophyre (~1.03), given that the model P_c value is 1.1.

The initial k_{a_n} direction expressed in reference coordinates is then transformed to its initial igneous fabric orientation:

$$k'_{a_n} = \mathbf{D}_v \cdot k_{a_n} \quad (7)$$

where $n = 1, 2, 3 \ldots 500$.

5.1.2. Superposed tectonic strain

The system of k_a orientations, representing the pure lineation of the granophyre, are rotated into orientations representing North and East Ranges, suitable for the superposition of tectonic strain (see Fig. 15). Plain strain shortening was applied in the orientation of the incremental strain ellipse illustrated in Fig. 15a, estimated from the tectonic strain fabrics of the Onaping Formation (Fig. 8). The incremental tectonic deformation matrix is given by:

$$\mathbf{D}_t = \begin{pmatrix} \frac{1}{0.99} & 0 & 0 \\ 0 & 1 & 0 \\ 0 & 0 & 0.99 \end{pmatrix}^N \quad (8)$$

where N is the number of deformation increments.

5.2. Results

The modelled AMS fabrics developed in the hypothetical North and East Ranges, at cumulative shortening strains of 5%, 10%, 15%, 30% and 50% (N = 5, 11, 17, 35 and 68, respectively), are illustrated in Fig. 15b. Mean magnetic foliation and lineation data are plotted from ten randomly generated data sets, each consisting of 500 grains with P_c values of 1.1. The strain history of one such data set, representing the East Range, is shown in Fig. 15a.

The hypothetical North Range plots indicate that only 5% strain is needed to displace the mean magnetic lineation 4° from its original position (Fig. 15b). At 10% cumulative strain the magnetic lineation is moved 10° away from its original position. The hypothetical East Range data indicates a slower migration of the magnetic lineation, but the magnetic foliation develops at a faster rate, and at 5% strain the magnetic foliation is well-defined (Fig. 15b). For the same amount of strain applied to the original virtual strain fabric, the development of the magnetic foliation, as a consequence of superposed tectonic strain, is the function of the orientation of the virtual lineation. As seen in the model North Lobe plots, the magnetic foliation develops most rapidly if the virtual lineation lies close to the X–Y plane of cumulative tectonic strain (Fig. 15b). This may be the reason why the magnetic foliation is well clustered in the East Range, but is poorly developed in the North Range (Fig. 8b).

The mean orientation of the magnetic lineation from domains B, C, D, E, G, H and I all indicate that they have not significantly moved from their original contact-orthogonal orientations (compare stereoplots of Fig. 15b to contoured magnetic lineation peaks and poles to estimated SIC contacts in Fig. 8a). A few of the magnetic lineations appeared to have moved form their original positions in domain F, if the dip of the contact is assumed to be dipping 60°–70° west along the eastern SIC contact. Nevertheless, the North Lobe does not appear to have been affected by *pervasive strain* since a well-defined contact-orthogonal lineation maximum is present in domain E (Fig. 8a). Using the AMS models as a guide-line (Fig. 15), the maximum shortening strains needed to explain the AMS fabric of the eastern granophyre is likely within 5% shortening for domains B, C, D, E, G, H and I, and within 15% shortening for domain F.

Strain estimates of above are applicable to the SIC provided that the intrinsic grain anisotropy P_c used in the modelling is consistent with the magnetic carriers of the granophyre. It is likely that these strain estimates are applicable if the magnetic grains of the granophyre are dominated by magnetite, which according to Borradaile et al. (1987) has a modest P_c value of ~1.18. Many other paramagnetic minerals, such as hornblende, have much greater P_c values

(~1.7 for hornblende) as well, and magnetites with higher P_c values would accordingly require much lower values of shortening strains to obtain the same AMS fabric patterns as illustrated in Fig. 15. For example, shortening strains of <5% are only needed for grains with $P_c > 1.3$ (with initial AMS ellipsoid

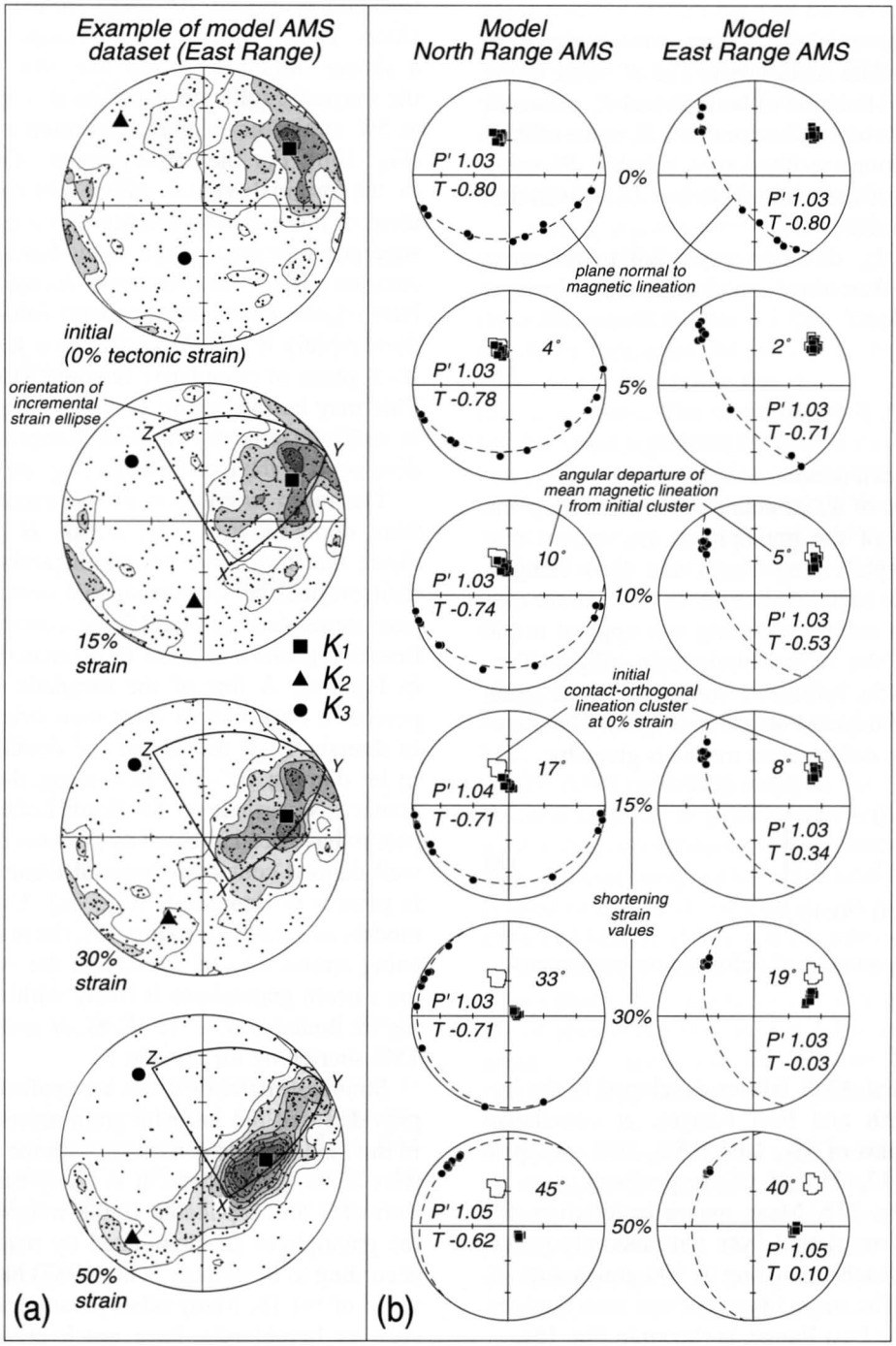

intensity of $P' = 1.04$), to obtain similar AMS patterns to those of 15% shortening predicted for $P_c = 1.1$ (Fig. 15b).

The susceptibility values of the SIC are quite variable and range over several orders of magnitude, and it was established that the ferrimagnetic contribution ranged from 0% to nearly 100% (Figs. 2 and 10b). This indicates that some samples would be entirely dominated by magnetite, as confirmed by thin-section examination, while others by paramagnetic mixtures of ilmenite, amphibole, chlorite and biotite. Although the dominant paramagnetic mineralogy was not investigated in samples with low ferrimagnetic contributions, the fact that almost identical AMS fabrics were obtained from contrasting magnetic carriers (with a variety of P_c values) suggest that the tectonic strain involved in the formation AMS fabrics of the granophyre may be relatively low. This interpretation is supported by the lack of pronounced solid-state deformation seen in the North Lobe (Fig. 13).

5.3. Strains expected from solid-state folding of an igneous sheet

The numerical simulation of AMS indicates that the contact-orthogonal AMS lineation of the granophyre is only slightly modified by tectonic strain. The results of the modelling are consistent with tectonic strain superposed on an already dipping SIC, i.e., basin-shaped igneous body, similar to the present geometrical configuration in the North and East Ranges (Fig. 15; Cowan et al., 1999, fig. 10a). Modelling estimates indicate possibly up to 15% strain in domain F, but solid-state strain is not pervasive in the North Lobe (Fig. 12). Thin-sections of samples obtained along the hinge of the North Lobe exhibit very low levels of solid-state strain (Fig. 13), more consistent with <5% strain.

In order to compare these strain estimates to strains expected in folds similar in geometry to that of the North Lobe, the interlimb angle of the North Lobe must be determined. The northern limb of the North Lobe dips approximately 40° toward 175°. The southeastern limb of the North Lobe dips 70° toward 265° (Rousell, 1984). Interlimb angle of the North Lobe is calculated to be 105° using these values and the plunge of the fold is 41/200. Down-plunge projection of the North Lobe (Fig. 12) using this plunge value is shown in Fig. 16a.

As the AMS modelling showed (Fig. 15), the initial orthogonality between the linear fabric element of the granophyre and the SIC contact will be destroyed if subjected to even minor tectonic shortening. This is particularly relevant to the North Lobe if its curvature formed by flexural folding. This fold mechanism seems unlikely because the mean magnetic lineation is approximately perpendicular to the basal contact of the SIC in all domains (Fig. 8a; Cowan et al., 1999, fig. 5), this fold mechanism seems unlikely. The orthogonality may, however, have been preserved during folding if strain axes were coaxial to the petrofabric, i.e., parallel to the axis of mineral alignment and the contact plane of the SIC such as by orthogonal flexure (Twiss and Moores, 1992, pp. 240–241). Folding strains associated with orthogonal flexure were determined (Fig. 16b) by assuming: (1) the neutral surface of the fold to lie in the median position with respect to the outer and inner fold arcs; and (2) the thickness of the limb and the folded arc to remain constant, implied by the geometry of the SIC at the North Lobe (cf. Schwerdtner, 1977; Cobbold, 1979). In such a fold model, a shortening strain of 33% is expected in the outer arc with stretch parallel to the contact, and 49% axial-planar shortening in the inner arc (Fig. 16b). Microstructural examination of host rocks revealed

Fig. 15. (a) AMS modelling, showing an example of computer-generated prolate *virtual* AMS fabric prior to tectonic deformation, oriented to simulate the East Range configuration, and showing the same data set after 15%, 30% and 50% cumulative shortening strains. Small dots represent long axes of 500 magnetic particles with P_c values of 1.1. Indicated orientation of the incremental strain ellipse was estimated from the tectonic fabric of the Onaping Formation from Fig. 8. The extension axis (X), intermediate axis (Y) and the shortening axis (Z) of the incremental strain ellipse plunges 60/150, 00/060, and 30/330, respectively. (b) Ten randomly generated data sets, similar to that shown in (a), are oriented into a hypothetical North Range and East Range orientations, with virtual extension plunges of 55/330 and 25/055, respectively. The initial fabrics were coaxially strained to 5%, 10%, 15%, 30% and 50% cumulative plane strains. Orientations of K_1 and K_3 are shown for these stages. The plane shown normal to the magnetic lineation (K_1) at 0% strain in both ranges (dashed great circle) is subparallel to the SIC basal contact at these localities.

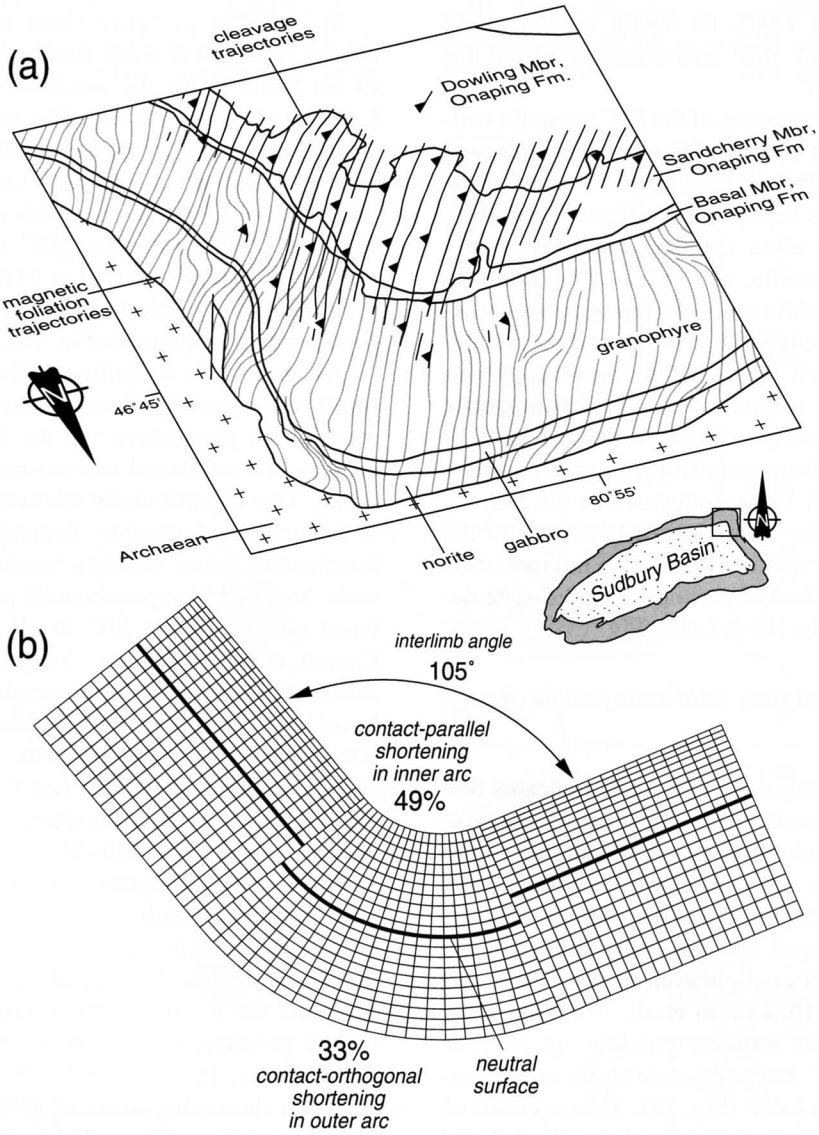

Fig. 16. (a) Down-plunge projection view of the North Lobe shown in Fig. 12. (b) Plane strain orthogonal flexure fold with the same interlimb angle as the North Lobe (105°). The outer arc must undergo layer-parallel stretch in order to preserve the orthogonality of lines, and conversely, axial-planar shortening in the inner arc. This layer-parallel stretch is absent from the North Lobe shown in (a). Strain levels are also incompatible between the North Lobe (a) and the fold model (b) as shortening of 49% and 33% are theoretically required in the inner and outer arcs, respectively, according to the fold model. Evidence for high levels of solid-state strain, however, is clearly lacking in the North Lobe (Fig. 13). Note that the orthogonal flexure model of (b) does not preserve continuity of strain from the limbs to the fold, although layer thickness is preserved.

only minor distortion of quartz by dislocation creep in quartz (Figs. 12 and 13), thus indicating a low level of solid-state overprint and is therefore inconsistent with high shortening strains expected from folding by orthogonal flexure in the North Lobe (Fig. 7b). In addition, the absence of layer-parallel stretching in the outer arc, but instead, the ubiquity of axial-planar magnetic foliation, negates the orthogonal flexure mechanism in the North Lobe (Fig. 16).

The tectonic lineation preserved in the Onaping Formation of the North Lobe indicates that the cumulative extension direction resulting from the tectonic deformation plunges to the south and southeast (see Onaping stereoplots of Fig. 8). This extension direction is subparallel to the plunge axis of the North Lobe (41/200), thus inconsistent with strains expected as a result of the North Lobe forming as a result of plane strain folding (e.g., Fig. 16b). The strains recorded in the Onaping Formation are instead consistent with regional strains associated with the South Range shear zone (Shanks and Schwerdtner, 1991), where stretch resulting from this thrust deformation is southeasterly plunging (Fig. 1b). The similarity of the observed AMS data with the model AMS results, assuming a southeasterly tectonic stretch (Figs. 8 and 15), indeed supports the hypothesis that the strains recorded in the Onaping Formation and the SIC are the result of regional strains associated with the South Range shear zone, and not strains resulting from local folding of the SIC in the North Lobe.

The magnetic fabric modelling of the SIC in the North and East Ranges (Fig. 15) is consistent with low levels of tectonic strain superposed on initially dipping SIC contacts. There are no known folding mechanisms that will yield the present fold-like geometry of the North Lobe without substantially altering the contact-orthogonal magnetic lineation fabric preserved in the granophyre. Fold origin for the North Lobe is also inconsistent with the orientation of the tectonic lineation recorded in the Onaping Formation. This rules out any emplacement models for the SIC, including the impact-melt model (Grieve et al., 1991), that require the consolidated SIC to have folded into the present basinal geometry from a horizontal sheet. Instead, it is likely that the SIC intruded along a bowl-shaped interface that was established as a result of the impact event (Cowan et al., 1999). The initially basin-shaped SIC was subsequently deformed to varying levels by the regional strains associated with the South Range shear zone (Fig. 1b).

6. Conclusions

The magnetic fabric study of the SIC in the North and East Ranges leads to the following conclusions.

(1) The AMS fabrics of the unstrained SIC consists of a contact-parallel magnetic foliation and a down-dip lineation in the gabbro–norite, and contact-orthogonal magnetic lineation and variable magnetic foliation in the granophyre.

(2) The magnetic fabrics of the gabbro–norite can be correlated with a triaxial igneous fabric. The magnetic lineation of the granophyre is correlated to a contact-orthogonal comb-layer (crescumulate) fabric, but the foliation could not be correlated to any physical silicate mineral fabric.

(3) The contact-orthogonal magnetic fabric of the granophyre is ubiquitous, except where substantial strain has destroyed this fabric in the South Range shear zone. The magnetic lineation is largely preserved in the East Range, North Range and in the North Lobe — the sharp fold-like juncture of the two ranges. The magnetic foliation of the granophyre is most strongly developed in the North Lobe where it is axial-planar in orientation, continuous with trajectories of the tectonic foliation of the adjacent Onaping Formation.

(4) The AMS anisotropy degree (P') in granophyre is commonly $<4\%$, therefore very small shortening strains will modify the contact-orthogonal magnetic lineation formed as a result of crescumulate crystallisation. A conservative estimate of shortening required to significantly modify this AMS fabric is $<15\%$ in the North Lobe, but is most likely $<5\%$ because of the preservation of contact-orthogonal magnetic lineation. Microscopic observations of the SIC samples from the North Lobe indicate very low strains, consistent with this interpretation.

(5) Contrary to the impact-melt model of the SIC (Grieve et al., 1991), the low strain level of rocks throughout the northern and eastern SIC suggests that it was not emplaced as a horizontal sheet, and subsequently folded after consolidation by solid-state deformation. Instead, the structural data are consistent with low levels of tectonic strain superposed on initially dipping SIC contacts. The basin-shaped contact surface of the Basal Onaping Formation and the basement rocks was likely acquired from the impact event, and the SIC intruded along this curved interface (Cowan et al., 1999).

Acknowledgements

This research was funded by an OGS Special Grant, and NSERC operating grants to W.M. Schwerdtner. Computer support and funding during the preparation of the manuscript was provided by the Tectonics Special Research Centre, University of Western Australia. Access to INCO Ltd. and Falconbridge Ltd. properties is gratefully acknowledged. Patrick Launeau and John Rucklidge are thanked for their technical expertise in the field of image analysis. Chris Hale and John Dehls are thanked for advice on the vibrating sample magnetometer study, and David Dunlop for the use of the VSM at Erindale Campus. Bill Morris of McMaster University kindly provided the drill equipment. This research greatly benefited from discussions with Keith Benn, Pierre Robin, Sandy Cruden, and Burkhard Dressler. Thoughtful comments by reviewers Frank Fueten and Pierre Rochette helped to significantly improve the paper. Professor W.M. (Fried) Schwerdtner suggested and supervised this project. I am indebted to him for his guidance, and for helpful discussions during the project. Lithoprobe publication number 1010.

References

Ames, D.E., Gibson, H.L., 1995. Controls on and geological setting of regional hydrothermal alteration within the Onaping Formation, footwall to the Errington and Vermilion base metal deposits, Sudbury Structure, Ontario. Geological Survey of Canada Current Research 1995_E, pp. 161–173.

Archanjo, C.J., Launeau, P., Bouchez, J.L., 1995. Magnetic fabric vs. magnetite and biotite shape fabrics of the magnetite-bearing granite pluton of Gameleiras (Northeast Brazil). Phys. Earth Planet. Inter. 89, 63–75.

Avermann, M., 1994. Origin of the polymict, allochthonous breccias of the Onaping Formation, Sudbury Structure, Ontario, Canada. In: Dressler, B.O., Grieve, R.A.F., Sharpton, V.L. (Eds.), Large Meteorite Impacts and Planetary Evolution. Special Paper, Geological Society of America, Boulder, CO, pp. 265–274.

Benn, K., 1994. Overprinting of magnetic fabrics in granites by small strains: numerical modelling. Tectonophysics 233, 153–162.

Benn, K., Rochette, P., Bouchez, J.L., Hattori, K., 1993. Magnetic susceptibility, magnetic mineralogy and magnetic fabrics in a late Archean granitoid-gneiss belt. Precambrian Res. 63, 59–81.

Borradaile, G., Keeler, W., Alford, C., Sarvas, P., 1987. Anisotropy of magnetic susceptibility of some metamorphic minerals. Phys. Earth Planet. Inter. 48, 161–166.

Borradaile, G.J., 1988. Magnetic susceptibility, petrofabrics and strain. Tectonophysics 156, 1–20.

Bouchez, J.L., 1997. Granite is never isotropic: an introduction to AMS studies of granitic rocks. In: Bouchez, J.L., Hutton, D.H.W., Stephens, W.E. (Eds.), Granite: From Segregation of Melt to Emplacement Fabrics. Kluwer, Dordrecht, pp. 95–112.

Carpenter, P.K., 1983. Origin of comb layering in the Willow Lake intrusion, N.E. Oregon. Geol. Soc. Am. Abstr. Progr. 15, 420.

Cintala, M.J., Grieve, R.A.F., 1994. The effects of differential scaling of impact melt and crater dimensions on lunar and terrestrial craters: some brief examples. In: Dressler, B.O., Grieve, R.A.F., Sharpton, V.L. (Eds.), Large Meteorite Impacts and Planetary Evolution. Special Paper, Geological Society of America, Boulder, CO, pp. 51–59.

Cobbold, P.R., 1979. Removal of finite deformation using strain trajectories. J. Struct. Geol. 1 (1), 67–72.

Cowan, E.J., 1996. Deformation of the Eastern Sudbury Basin. Ph.D. Thesis, University of Toronto, Toronto.

Cowan, E.J., Schwerdtner, W.M., 1994. Fold origin of the Sudbury Basin. In: Lightfoot, P.C., Naldrett, A.J. (Eds.), Proceedings of the Sudbury–Noril'sk Symposium. Special Volume, Ontario Geological Survey, Toronto, pp. 45–55.

Cowan, E.J., Riller, U., Schwerdtner, W.M., 1999. Emplacement geometry of the Sudbury Igneous Complex: structural examination of a proposed impact melt sheet. In: Dressler, B.O., Sharpton, V.L. (Eds.), Meteorite Impacts and Planetary Evolution II. Special Paper, Geological Society of America, Boulder, CO 333, in press.

Cruden, A.R., Launeau, P., 1994. Structure, magnetic fabric and emplacement of the Archean Lebel Stock, SW Abitibi Greenstone Belt. J. Struct. Geol. 16 (5), 677–691.

Dietz, R.S., 1964. Sudbury Structure as an astrobleme. J. Geol. 72, 412–434.

Dietz, R.S., Butler, L.W., 1964. Shatter-cone orientation at Sudbury, Canada. Nature 204, 280–281.

Dressler, B.O., 1987. Precambrian geology of the Falconbridge Township, District of Sudbury. Ontario Geological Survey, Toronto.

Dressler, B.O., Gupta, V.K., Muir, T.L., 1991. Chapter 15: The Sudbury Structure. In: Thurston, P.C., Williams, H.R., Sutcliffe, R.H., Stott, G.M. (Eds.), Geology of Ontario. Special Volume, Ontario Geological Survey, Toronto, pp. 593–625.

Dressler, B.O., Weiser, T., Brockmeyer, P., 1996. Recrystallized impact glasses of the Onaping Formation and the Sudbury Igneous Complex, Sudbury Structure, Ontario, Canada. Geochim. Cosmochim. 60 (11), 2019–2036.

Ellwood, B.B., Whitney, J.A., 1980. Magnetic fabric of the Elberton Granite, northeast Georgia. J. Geophys. Res. 85 (B3), 1481–1486.

Faggart, B.E., Basu, A.R., Tatsumoto, M., 1985. Origin of the Sudbury Complex by meteoritic impact: neodymium isotropic evidence. Nature 230, 436–439.

Grieve, R.A.F., Stöffler, D., Deutsch, A., 1991. The Sudbury

Structure: controversial or misunderstood? J. Geophys. Res. 96 (E5), 22753–22764.

Guillet, P., Bouchez, J.-L., Wagner, J.-J., 1983. Anisotropy of magnetic susceptibility and magmatic structures in the Guerande Granite Massif (France). Tectonics 2, 419–429.

Hamilton, W., 1960. Form of the Sudbury Lopolith. Can. Mineral. 6, 437–447.

Hext, G.R., 1963. The estimation of second-order tensors, with related tests and design. Biometrika 50, 353–373.

Hrouda, F., 1982. Magnetic anisotropy of rocks and its application in geology and geophysics. Geophys. Surv. 5, 37–82.

Jelinek, V., 1978. Statistical processing of anisotropy of magnetic susceptibility measured on groups of specimens. Stud. Geophys. Geod. 22, 50–62.

Krogh, T.E., Davis, D.W., Corfu, F., 1984. Precise U–Pb zircon and baddeleyite ages for the Sudbury area. In: Pye, E.G., Naldrett, A.J., Giblin, P.E. (Eds.), The Geology and Ore Deposits of the Sudbury Structure. Special Volume, Ontario Geological Survey, Toronto, pp. 431–446.

Krogh, T.E., Kamo, S.E., Bohor, B.F., 1996. Shock metamorphosed zircons with correlated U–Pb discordance and melt rocks with concordant protolith ages indicate an impact origin for the Sudbury Structure. Earth Processes: Reading the Isotopic Code. American Geophysical Union, Washington, DC, pp. 343–353.

Kruhl, J.H., 1996. Prism- and basal-plane parallel subgrain boundaries in quartz: a microstructural geothermobarometer. J. Metamorph. Geol. 14, 581–589.

Lakomy, R., 1990. Implications for cratering mechanics from a study of the Footwall Breccia of the Sudbury impact structure, Canada. Meteoritics 25, 195–207.

Launeau, P., Robin, P.-Y.F., 1996. Fabric analysis using the intercept method. Tectonophysics 267, 91–119.

Launeau, P., Cruden, A.R., Bouchez, J.-L., 1994. Mineral recognition in digital images of rocks: a new approach using multichannel classification. Can. Mineral. 32, 919–933.

March, A., 1932. Mathematische Theorie der Regelung nach der Korngestalt bei affiner Deformation. Z. Kristallogr. 81, 285–297.

McBirney, A.R., Noyes, R.M., 1979. Crystallization and layering of the Skaergaard Intrusion. J. Petrol. 20 (3), 487–554.

Milkereit, B., Green, A., The Sudbury Working Group, 1992. Geometry of the Sudbury Structure from high-resolution seismic reflection profiling. Geology 20, 807–811.

Moore, J.G., Lockwood, J.P., 1973. Origin of comb layering and orbicular structure, Sierra Nevada Batholith, California. Geol. Soc. Am. Bull. 84, 1–20.

Muir, T.L., 1984. The Sudbury Structure; considerations and models for an endogenic origin. In: Pye, E.G., Naldrett, A.J., Giblin, P.E. (Eds.), The Geology and Ore Deposits of the Sudbury Structure. Special Volume, Ontario Geological Survey, Toronto, pp. 449–490.

Naldrett, A.J., Hewins, R.H., 1984. The main mass of the Sudbury Igneous Complex. In: Pye, E.G., Naldrett, A.J., Giblin, P.E. (Eds.), The Geology and Ore Deposits of the Sudbury Structure. Special Volume, Ontario Geological Survey, Toronto, pp. 235–251.

Nicolas, A., 1992. Kinematics in magmatic rocks with special reference to gabbros. J. Petrol. 33 (4), 891–915.

Nye, J.F., 1985. Physical Properties of Crystals. Oxford University Press, Oxford, 329 pp.

Owens, W.H., 1974. Mathematical model studies on factors affecting the magnetic anisotropy of deformed rocks. Tectonophysics 24, 115–131.

Peredery, W.V., 1972. Chemistry of fluidal glasses and melt bodies in the Onaping Formation. In: Guy-Bray, J.V. (Ed.), New Developments in Sudbury Geology. Special Paper, Geological Association of Canada, Toronto, pp. 49–59.

Peredery, W.V., Morrison, G.G., 1984. Discussion of the origin of the Sudbury Structure. In: Pye, E.G., Naldrett, A.J., Giblin, P.E. (Eds.), The Geology and Ore Deposits of the Sudbury Structure. Special Volume, Ontario Geological Survey, Toronto, pp. 491–512.

Peredery, W.V., Naldrett, A.J., 1975. Petrology of the upper irruptive rocks, Sudbury, Ontario, Canada. Econ. Geol. 70, 164–175.

Quadling, K., Cawthorn, R.G., 1994. The layered Gabbronorite Sequence, Main Zone, eastern Bushveld Complex. S. Afr. J. Geol. 97 (4), 442–454.

Richter, C., 1992. Particle motion and the modelling of strain response in magnetic fabrics. Geophys. J. Int. 110, 451–464.

Richter, C., van der Pluijm, B.A., 1994. Separation of paramagnetic and ferrimagnetic susceptibilities using low temperature magnetic susceptibilities and comparison with high field strengths. Phys. Earth Planet. Inter. 82 (2), 113–123.

Richter, C., Ratschbacher, L., Frisch, W., 1994. Reply to comment on 'Magnetic fabrics, crystallographic preferred orientation, and strain of progressively deformed metamorphosed pelites in the Helvetic zone of the Central Alps (Quatenschiefer Formation)' by C. Richter, L. Ratschbacher and W. Frisch. J. Geophys. Res. 99 (B11), 21829–21831.

Robin, P.-Y.F., 1977. Determination of geologic strain using randomly oriented strain markers. Tectonophysics 42, T7–T16.

Robin, P.-Y.F., Jowett, E.C., 1986. Computerized density contouring and statistical evaluation of orientation data using counting circles and continuous weighting functions. Tectonophysics 121, 207–223.

Rochette, P., 1987. Magnetic susceptibility of the rock matrix related to magnetic fabric studies. J. Struct. Geol. 9, 1015–1020.

Rochette, P., 1994a. Comment on 'Magnetic fabrics, crystallographic preferred orientation, and strain of progressively deformed metamorphosed pelites in the Helvetic zone of the Central Alps (Quatenschiefer Formation)' by C. Richter, L. Ratschbacher, and W. Frisch. J. Geophys. Res. 99 (B11), 21825–21827.

Rochette, P., 1994b. Comments on 'Anisotropic magnetic susceptibility in the continental lower crust and its implication for the shape of magnetic anomalies' by G. Florio, M. Fedi, A. Rapolla, D.M. Fountain and P.N. Shive. Geophys. Res. Lett. 21, 2773–2774.

Rousell, D.H., 1984. Structural geology of the Sudbury Basin. In: Pye, E.G., Naldrett, A.J., Giblin, P.E. (Eds.), The Geology

and Ore Deposits of the Sudbury Structure. Special Volume, Ontario Geological Survey, Toronto, pp. 83–95.
Schwerdtner, W.M., 1977. Geometric interpretation of regional strain analyses. Tectonophysics 39, 515–531.
Shanks, W.S., Schwerdtner, W.M., 1991. Structural analysis of the central and southwestern Sudbury Structure, Southern Province, Canadian Shield. Can. J. Earth Sci. 28, 411–430.
Spray, J.G., Thompson, L.M., 1995. Friction melt distribution in a multi-ring impact basin. Nature 373, 130–132.
Tarling, D.H., Hrouda, F., 1993. The Magnetic Anisotropy of Rocks. Chapman and Hall, London, 217 pp.
Twiss, R.J., Moores, E.M., 1992. Structural Geology. W.H. Freeman, New York, 532 pp.
Vollmer, F.W., 1990. An application of eigenvalue methods to structural domain analysis. Geol. Soc. Am. Bull. 102, 786–791.